Desalination and Water Treatment
www.deswater.com
doi: 10.5004/dwt.2020.25451

187 (2020) 345–369
May

Adsorption performances and antimicrobial activity of the nanosilver modified montmorillonite clay

Maja Stevanović[a], Zoran J. Bajić[b], Zlate S. Veličković[b], Radovan M. Karkalić[b], Ljiljana Pecić[c], Pavel Otřísal[d], Aleksandar D. Marinković[e,*]

[a]*Innovation Center of the Faculty of Technology and Metallurgy in Belgrade Ltd., University of Belgrade, Belgrade, Serbia*
[b]*The Military Academy, University of Defense, 33 General Pavle Jurišić–Šturm street, 11000 Belgrade, Serbia*
[c]*Technical College of Applied Studies in Mechanical Engineering Trstenik, 19 Radoja Krstića street, 37240 Trstenik, Serbia*
[d]*University of Defense, NBC Defense Institute, Víta Nejedlého, 682 01 Vyškov, Czech Republic*
[e]*Faculty of Technology and Metallurgy, University of Belgrade, Karnegijeva 4, 11120 Belgrade, Serbia,*
email: marinko@tmf.bg.ac.rs (A.D. Marinković)

Received 17 June 2019; Accepted 8 January 2020

ABSTRACT

The synthesis and adsorption potential of Cy-npAg, obtained by modification of raw montmorillonite clay (raw-Cy) with silver nanoparticle (npAg), was studied in this work. Optimization procedure, with respect to time, temperature and amount of deposit npAg, obtained either by reductive precipitation or ultraviolet irradiation, was performed using response surface methodology (RSM). The most efficient adsorbent, obtained by chemical reduction of silver ion with sodium borohydride, named Cy-npAg, was characterized in detail using Brunauer-Emmett-Teller, scanning electron microscopy, Fourier transform infrared spectroscopy and X-ray diffraction techniques, and point of zero charge determination. The Cy-npAg showed good adsorption capacity with respect to non-systemic organophosphate insecticide (diazinon) as well as of heavy metals ions (Cd^{2+} and Ni^{2+} ions), that is, 74.26, 62.33, and 35.49 mg g^{-1}, respectively, obtained from Langmuir model fitting. Temperature dependent kinetic study allowed determination of pseudo-second rate constant (10^3 g mg^{-1} min^{-1})/activation energies (kJ mol^{-1}): 1.45/14.48 for diazinon, and 1.27/6.59 and 0.7/7.35 kJ mol^{-1} for Cd^{2+} and Ni^{2+} ions, respectively. Thermodynamic parameters indicated feasible and spontaneous adsorption with main participation of physisorption. Antibacterial potential of npAg deposit for water disinfection was confirmed by the moderate reduction of bacterial growth of *Staphylococcus aureus*, *Escherichia coli*, and *Pseudomonas aeruginosa*, by 64%, 39%, and 70%, respectively. Thus, two synergistic effects contribute to water purification processes using Cy-npAg: pollutants removal with a simultaneous decrease of the microbial contamination contributing to overall water quality improvement.

Keywords: Diazinon; Heavy metal; Clay; Silver nanoparticle; Antibacterial properties

1. Introduction

There is an increasing demand for the development of efficient and economic adsorbents for the treatment of wastewater that is capable to remove removal toxic or hazardous organic contaminants, heavy metals, and pathogenic microorganisms. Wastewaters contaminated with heavy metals, organic pollutants, and pathogenic microorganisms pose a serious risk to public health and important issue of environmental protection.

Heavy metals are toxic, non-biodegradable, and can bio-accumulative in living organisms [1], usually entering

* Corresponding author.

the human body through water, food, or air [1–4]. Organic pollutants such as pesticides and herbicides are increasingly present in wastewater. The most common is the origin of industrial production. Pesticides and herbicides are life-threatening due to their toxicity, carcinogenicity, and mutagenicity [5]. The origin of pathogenic microorganisms in wastewater is from human excretions in communal waters and wastewater from industries such as slaughterhouses. Viruses and bacteria can cause diseases that are transmitted by water, such as cholera, typhoid, dysentery, polyol, and infectious hepatitis in humans. Thus, the presence of hazardous contaminants: heavy metal, pesticides and their degradation products, and pathogens in water demand application of appropriate technologies/processes able to perform their removal/degradation to provide a concentration in the effluent under value recommended by World Health Organization recommendations (WHO).

Decreasing trend of maximum allowable content of heavy metal ions/pesticides in natural and wastewater forced the development of improved technologies for their effective removal. Various treatment methods such as ultrafiltration, ion exchange, coagulation/precipitation, membrane filtration, reverse osmosis, electrolysis, oxidation, and photodegradation and adsorption have been used for wastewater purification [2,6,7]. Except for many advantageous characteristics these technologies have some disadvantages such as low efficiency and economic viability. Among them, adsorption is cheap, efficient, and easily adaptable technique, and thus could be widely used for the removal of pollutants from water [4,8–14]. In recent years, a huge amount of work was devoted to the development of selective and efficient adsorbent obtained by precipitation of the structurally arranged nanoparticle on the support of the natural origin.

Minerals from the group aluminosilicate are very present in the Earth's crust, including the most important mineral clay in this group that can be used for the adsorption process. These minerals contain a layered structure. Between layers of crystal gratings, there are cations that can easily be replaced. The layered clay structures also integrate water that is placed around its cations or left in free form. As clay is a polar substance, polar organic molecules can be installed in the layered structure, either by being adsorbed physically or through chemisorption, to bind to the active site. Clay is potentially an effective adsorbent which is chemically and mechanically stable. Its high specific surface area, high cation exchange capacity of its layered structure in which nanoparticle materials can be easily doped to improve the characteristics of the adsorbent also make it a potentially effective adsorbent. Moreover, all of these properties make clay a useful adsorbent which can adsorb various metal ions, inorganic anions, and organic ligands. Its wide distribution, positive adsorption features, and low price make it stand out in its efficient use for removal of heavy metals from water as an adsorbent [4,11]. In previous studies, disparate varieties of clays to remove various pollutants from the water, including highly toxic organic substances [15,16], oils and fats [17,18], and heavy metals [4,19–29] were used.

Precipitation of nanosized particles, for example, silver nanoparticles (npAg), on montmorillonite (raw-Cy) supports could improve adsorbent performance: textural properties, adsorptive and kinetic performances, and combining antimicrobial effect in the course of water purification. Previous results have shown that npAgs, with known antimicrobial properties [30–32], also contributed to the improved adsorption of pesticides (diazinon) and Cd^{2+} and Ni^{2+} cations for 47%, 25%, and 19%, respectively. Thus, the main goal of the research was focused on the development of an optimal method for the simultaneous reduction/precipitation of npAg on natural raw-Cy in order to improve the adsorption and antimicrobial properties of newly synthesized Cy-npAg adsorbent. Two processes of npAg deposition were considered: classic chemical reduction using sodium borhydride, Cy-npAg$_{Ch}$ named adsorbent, and photochemical method, Cy-npAg$_{Ph}$ named adsorbent. The response surface methodology (RSM) was used in an optimization process of the adsorbents syntheses, considering adsorption capacity of diazinon removal in relation to synthesis parameters (temperature, reaction time, and the amount of the deposited silver) [33,34]. Box-Behnken three-factor rotatable designs were applied for the adsorption capacity of diazinon as the response. This design was successfully used in studies dealing with adsorbent synthesis [35] and adsorption process experiments [36].

2. Experimental

Batch adsorption study was used to examine the adsorption properties about the synthesis method [37,38]. The influence of the number of doped npAgs and other parameters (adsorbent mass, pH value, adsorption time, and adsorption temperature) on the adsorption capacity were studied. Adsorbent with the best adsorption capacity for diazinon, Cd^{2+}, and Ni^{2+} cations was characterized using various methods and techniques, that is, Brunauer-Emmett-Teller (BET), X-ray fluorescence (XRF), Fourier transform infrared spectroscopy (FTIR), X-ray diffraction (XRD), and scanning electron microscopy (SEM). Specific objectives of this study were focused on: (i) preparation of Cy-npAg with optimal adsorption properties, (ii) structural and morphological characterization of Cy-npAg, (iii) determination of kinetic and activation parameters, (iv) adsorption isotherm and thermodynamic parameters determination, (v) competitive adsorption and kinetic study, and (vi) evaluation of antimicrobial properties using microorganisms usually found in the waste water.

2.1. Materials

The information about materials used is given in the Supplementary material (part 1.1).

2.2. Adsorbent preparation and optimization procedure

Different modification procedures for the montmorillonite has been studied and described in the literature. However, the key reaction parameters should be investigated and selected carefully to perform the adequate design of experiments and optimization procedures. According to the previous research [15,16,19,26,32,37,39–42] the key variables are as follows:

- Concentration of the silver nitrate ($AgNO_3$) aqueous solution,

- Concentration of the reducing agent (sodium borohydride, $NaBH_4$),
- Reaction time and temperature, and

Method applied to obtain a uniform distribution of nanoparticles Ag (npAg) deposit.

The method for reduction of silver ion to elementary nanodeposited Ag (npAg) on raw-Cy was carried out in two ways: (1) chemical reduction and (2) photochemical deposition of npAg onto raw-Cy. Optimization of npAgs loading on raw-Cy support was performed with the intention to produce a high-performance adsorbent applicable in the removal of heavy metal ions and organic pollutants. The amount of $AgNO_3$ was calculated according to stoichiometry and the expected theoretical deposition of npAg (Table 1).

General procedure for chemically induced npAg deposition (CID): classical reduction of a silver ion with $NaBH_4$ was performed to obtained npAg/montmorillonite adsorbent (Cy-npAg$_{Ch}$; Ch, designate chemical reduction of silver ion) [37,38]. The theoretical amount of $AgNO_3$ solution (in mL, 2.5 mg mL^{-1}) was calculated to obtain 1, 3, and 5 wt.% of npAg on raw-Cy (Table 1). In typical experiments, 40 mL of the $AgNO_3$ solution (3.94 mg mL^{-1} $AgNO_3$; 2.5 mg mL^{-1} Ag) was mixed with the montmorillonite (10 g) at 200 rpm for a period of 2 h. After this step, 35.72 mL of the $NaBH_4$ aqueous solution (1.75 mg mL^{-1}) was added to suspension obtained according to Exp. 1 (Table 1), and the solution was mixed for 30 min at 298°K (Table 1). Finally, the obtained products were subjected to centrifugation, washed three times with deionized water (3 × 80 mL), filtered, and dried in vacuum at 353°K for 6 h. All other syntheses were performed in accordance with the plan given in Table 1.

General procedure for ultraviolet (UV) irradiation-induced npAg deposition on raw-Cy has been explained in the supplementary material.

To perform the full analysis of the influences of synthesis parameters on adsorbent properties, RSM was applied for both cations and diazinon removal, and obtained results were exemplified for diazinon (Supplementary material, part 1.2). According to the obtained results (part 3.1), CID method gave a better result, and due to appropriate inhomogeneity of npAg deposit on raw-Cy additional optimization was performed.

Improvement of the optimized method of Cy-npAg$_{Ch}$ synthesis is given in the Supplementary material.

2.3. Characterization and pollutant determination methods

Synthesized adsorbents were characterized using BET, XRF, FTIR, XRD, and SEM techniques and point of zero charge (pH_{PZC}), and detail on characterization methods are provided in Supplementary material, part 1.4. The concentration of diazinon was analyzed using ultraviolet-visible spectrophotometry (UV-VIS) spectrophotometry and high-performance liquid chromatography, while heavy metal ions by using inductively coupled plasma mass spectrometry (Supplementary material, part 1.4).

2.4. Adsorption and kinetic experimental conditions, and error functions

The adsorption of diazinon and heavy metal ions, Cd^{2+} and Ni^{2+} were studied in a batch system as it was described in recent studies [10,40,41]. More details on the conditions of adsorption are given in Supplementary material (part 1.5).

2.5. Antimicrobial activity

Sample was tested for antimicrobial properties in the direct contact on agar plates and in the suspension. In the direct contact, it was placed on the surface of the agar plates inoculated with *Staphylococcus aureus* ATCC29213, *Escherichia coli* ATCC 25922, and *Pseudomonas aeruginosa* ATCC 15442, according to the previously conducted study [38]. Detail on antimicrobial experiments is given in Supplementary material (part 1.6).

2.6. Modeling of ionic speciation

Method applied for modeling of ionic speciation is given in Supplementary material (part 1.7).

2.7. Modeling of diazinon structure

Method applied for modeling of ionic speciation is given in Supplementary material (part 1.8).

3. Results and discussion

3.1. Optimization of adsorbent synthesis

In several previous studies, it has been proven that metal ions possess a different affinity for the active sites present at the adsorbent surface [43]. Generally, the numbers of reactions that occur in a suspension at its solid-liquid boundary facilitate the adsorption of ions and molecules on the surface of the clay, that is, the adsorbent. The processes of adsorption and ion exchange are the predominant forms of removing heavy metal ions from a solution due to the different

Table 1
Theoretical amount of Ag in the adsorbent and the required $AgNO_3$ solution quantity for the preparation of Cy-npAg adsorbent

Experiments*	Adsorbent	Theoretical amount of Ag (%)	Required $AgNO_3$ solution (mL)	Concentration of Ag (mg mL^{-1})
1	Cy-npAg–1	1	40	2.5
2	Cy-npAg–3	3	120	2.5
3	Cy-npAg–5	5	200	2.5

*Chemical deposition of npAg was performed for 30, 60, or 90 min at temperatures 298°K, 323°K, or 348°K; deposition of npAg exerted by UV irradiation was performed for 60 min at room temperature.

functionalities of clay materials, which include: the range of the acidic sites, oxygen containing functionalities, and hydroxyl groups, which are mainly found on edges of crystal lattices [28].

Ion exchange characteristics, adsorption capacity, and kinetics of the clay-based adsorbent are dependent on the structure/properties of material deposited and the synthesis method applied. Thus, in the preliminary experiments related to the selection of the reduction process chemical reduction (Ch), about UV irradiation (Ph) showed higher efficiency of silver ion transformation to npAg.

Graphical representation of the results of detail optimization of the Cy-npAg$_{Ch}$ synthesis with the output variable, that is, the adsorption capacity of diazinon, for the amount of initial silver solution, time, and temperature are given in Fig. 1. Graphical area with intense red color designates regions that meet critical properties, while the regions without optimization criteria are snap-off. More precise optimization conditions are obtained by point prediction through the software based on the factors or components included in the model. The expected responses and associated trust intervals are calculated based on the prediction equation displayed at the analysis of variance output.

According to the results given in Fig. 1, as an operational parameters temperature of 70°C (343°K) and a reduction time of 60 min in further experiments of Cy-npAg$_{Ch}$ adsorbent synthesis was selected. On the basis of preliminary adsorption results using adsorbents Cy-npAg$_{Ch}$–1, Cy-npAg$_{Ch}$–3, and Cy-npAg$_{Ch}$–5 (Table 1) for a further research Cy-npAg$_{Ch}$–5 adsorbent was selected as the most efficient adsorbent (15%–65% for Cd^{2+} and 22%–78% for Ni^{2+} higher capacity with respect to Cy-npAg$_{Ch}$–1 and Cy-npAg$_{Ch}$–3), and 16% for Cd^{2+} and 20% for Ni^{2+} higher capacity than Cy-npAg$_{Ph}$. Also, comparative tests indicated that the adsorption capacities of unmodified clay were significantly lower in comparison to Cy-npAg$_{Ch}$–5: 24%–42% for Ni^{2+} and Cd^{2+}, and 29%–35% for diazinon. In order to further optimize synthesis procedure two methodologies of Cy-npAg$_{Ch}$ adsorbent synthesis were applied:

- adaptation of method by alternating portion-wise addition of $AgNO_3$ solution followed by reductive agent solution divided into three portions,
- study of the effect of drying method: vacuum or freeze drying methods after whole cycle of npAg deposition [Cy-npAg$_{Ch}$(FD)] or step-wise freeze drying [Cy-npAg$_{Ch}$(FD–3) showed that one pot freeze drying, after whole deposition procedure, gave a 7%–9% higher capacity of Cy-npAg$_{Ch}$(FD)].

The optimal adsorption performance was obtained by a controllable reduction of silver ion to provide 4.8 wt.% of npAg deposit in Cy-npAg$_{Ch}$–5. The results presented in the subsequent text relate to this material, named Cy-npAg$_{Ch}$. In an analogous manner, synthesis of Cy-Ag^+ adsorbent was performed by Na/Ag^+ ion-exchange process, at experimental condition applied for Cy-npAg$_{Ch}$-5 synthesis, but without addition of $NaBH_4$. This material was used in adsorption and antibacterial study, and obtained results were used for comparative purposes. Full detail on statistical analysis related to the optimization procedure is given in Supplementary material (part 2.1). Except for this, the application of the Silar method [44] did not give any comparable improvement. Generally, the presented results highlight the significance of the application of optimization procedure to obtain desirable material performances at the lowest number of experiments performed.

3.2. Physical and chemical characterization of the adsorbent

Surface properties and physical properties of the adsorbent are given in Table 2. The change of pH_{PZC} was influenced by the change of surface properties due to silver oxide nanoparticles deposition (Table 2). Low pH_{PZC} values of both adsorbents indicate that at pH > pH_{PZC} negatively charged adsorbent surface could be a driving force for cation attraction. Also, the decrease of pH_{PZC} value after adsorption, from 5.64 to 5.48 indicates the contribution of specific adsorption plays an appropriate role in an overall adsorption mechanism.

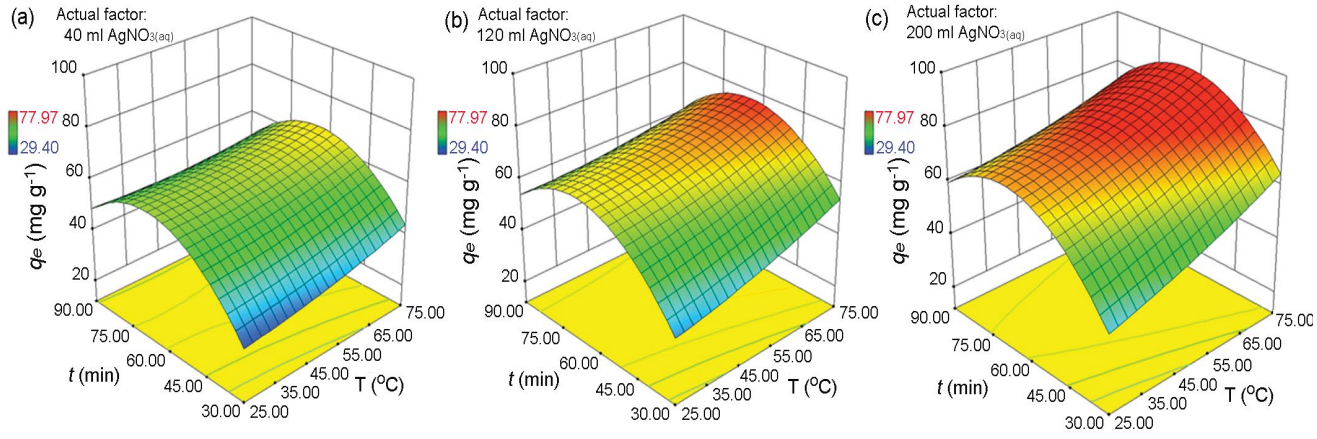

Fig. 1. Contour diagram representing relation between capacity q_e vs. t and T for Cy-npAg$_{Ch}$: (a) 40 mL, (b) 120 mL, and (c) 200 mL of $AgNO_3$ solution (in accordance to Table S1) ($C_{i[Diazinon]}$ = 30.00 mg L^{-1} and m/V = 200 mg L^{-1}) used in a optimization of Cy-npAg synthesis.

Table 2
Textural properties and pH_{PZC} of raw-Cy and Cy-$npAg_{Ch}$ adsorbents

Adsorbent	Specific surface area ($m^2\ g^{-1}$)	Pore volume ($mL\ g^{-1}$)	Pore diameter (nm)	pH_{PZC}*
raw-Cy	47.6	0.152	5.09	4.90
Cy-$npAg_{Ch}$	55.4	0.202	12.40	5.64

Appropriate increase of specific surface area and pore volume was, and significant increases of pore diameter were observed after raw-Cy modification with npAg. The results on the chemical constitution before and after modification, that is, raw-Cy and Cy-$npAg_{Ch}$, respectively, are given in Table S3. Full details on XRF of adsorbents are provided in Supplementary material (part 2.2). Also, their chemical content of raw-Cy, before and after modification with npAg, is compared to clays from other worldwide studies (Table S3).

3.3. Characterization of adsorbent functionalities–FTIR analysis

Detail on FTIR characterization of synthesized adsorbent Cy-$npAg_{Ch}$ and raw-Cy are given in Supplementary material (part 2.3).

3.4. XRD analysis

The XRD patterns of the raw-Cy and Cy-$npAg_{Ch}$ adsorbents are displayed in Fig. 2.

Raw-Cy contains an appropriate amount of siliceous impurity which produces intense peaks, even in small quantities. As shown in Fig. 2, the clay used is not pure montmorillonite, because the most intense peak is recorded at $2\theta = 26.7°$, due to the presence of quartz crystal. The XRD peaks of Cy-$npAg_{Ch}$ observed at 2θ of 38.25°, 44.25°, and 64.70° could be attributed to the (111), (200), and (220) crystallographic planes of the face-centered cubic silver crystals, respectively. A Significant decrease of the peak at $2\theta = 26.7°$ in all npAg modified samples could be a result of the purification procedure. For all samples, the main crystalline deposited phase was silver as no other impurities were found in the XRD patterns. The intensities of (111), (200), and (220) reflections, due to the npAg crystalline phase, were of the highest intensity in Cy-$npAg_{Ch}$. Similar results were published in relevant literature with main npAg peaks without the presence of other impurity [15,29,37,38,42,45]. The XRD patterns of the Cy-$npAg_{Ph}$ adsorbent, shown in part 2.4 of Supplementary material, reflect lower amount of deposited npAg and thus lower changes of diffraction pattern with respect to XRD of raw-Cy sample [6].

3.5. SEM analysis

The morphology and structure of raw-Cy and Cy-$npAg_{Ch}$ were studied using SEM microscopy. The representative images are shown in Fig. 3. The similar morphologies of both materials raw-Cy and Cy-$npAg_{Ch}$ could be noticed from Figs. 3a and c at lower magnification. The coarse structure of raw-Cy (Figs. 3a and b) was similar to Cy-$npAg_{Ch}$ (Fig. 3c), while at higher magnification (Fig. 3d) the morphology is significantly different due to precipitation of cluster like silver nanodeposit [37].

3.6. Effect of pH on the adsorption of the diazinon and Cd^{2+} and Ni^{2+} ions

Except for the adsorption conditions under which experiments are carried out two additional factors play a significant role in the adsorption process: Cd^{2+} and Ni^{2+} ion speciation and charge distribution over molecular orbitals of diazinon. Thus, the ionic speciation and molecular electrostatic potential (MEP) surface of diazinon, obtained using Minteq and MOPAC software package (Supplementary material, parts 1.7 and 1.8), was given on Figs. S3 and S4, respectively. These factors were further included in consideration of their influence on adsorption efficiency.

Influence of pH on the Cd^{2+} and Ni^{2+}, and diazinon adsorption on the Cy-$npAg_{Ch}$ is shown in Fig. S5. At a pH lower than 9, the dominant species of cadmium is Cd^{2+} and Ni^{2+}, present in the form of $[M(H_2O)_6]^{2+}$ [10]. At higher pH values, Cd^{2+} and Ni^{2+} ions create insoluble hydroxide rather susceptible to precipitation [46]. For this reason, the pH between 6 and 6.5 was taken as operative value at which cation adsorption was performed (Fig. S5). At pH < 6 slight increases of the adsorption of Ni^{2+} were noticed, while thereafter become nearly constant with pH increase. The lower adsorption efficiencies of both cations at lower pH could be the result of the electrostatic repulsion between the positively charged surface of the adsorbent (Table 3) and Cd^{2+} and Ni^{2+} ions in the solution, which hinders the process of metal bonding [47]. Preliminary studies of diazinon adsorption have shown that pH has a negligible effect on its adsorption process in the pH region 5–9, and thus pH 6 was selected as the optimal.

3.7. Effect of the contact time on the adsorption of diazinon, Cd^{2+}, and Ni^{2+} ions

In the first adsorption period (45 min) the adsorption of diazinon and Cd^{2+} onto Cy-$npAg_{Ch}$ was a relatively fast process, while it is somewhat slower for Ni^{2+} ion. During this period, about 80% of 85%, 94% of 97%, and 61% of 96% of total removal of diazinon, Cd^{2+}, and Ni^{2+} ions were obtained, respectively (Fig. S7). After that slow decreases of adsorption rate to the system, equilibration takes place. In the initial stage of adsorption, a large number of vacant surface sites are available for adsorption. Repulsive forces between the similarly charged solute molecules bonded to the solid and one approaching from bulk phases. Equilibrium was achieved almost within 90 min for diazinon and Cd^{2+} ion and 120 min for Ni^{2+} ions.

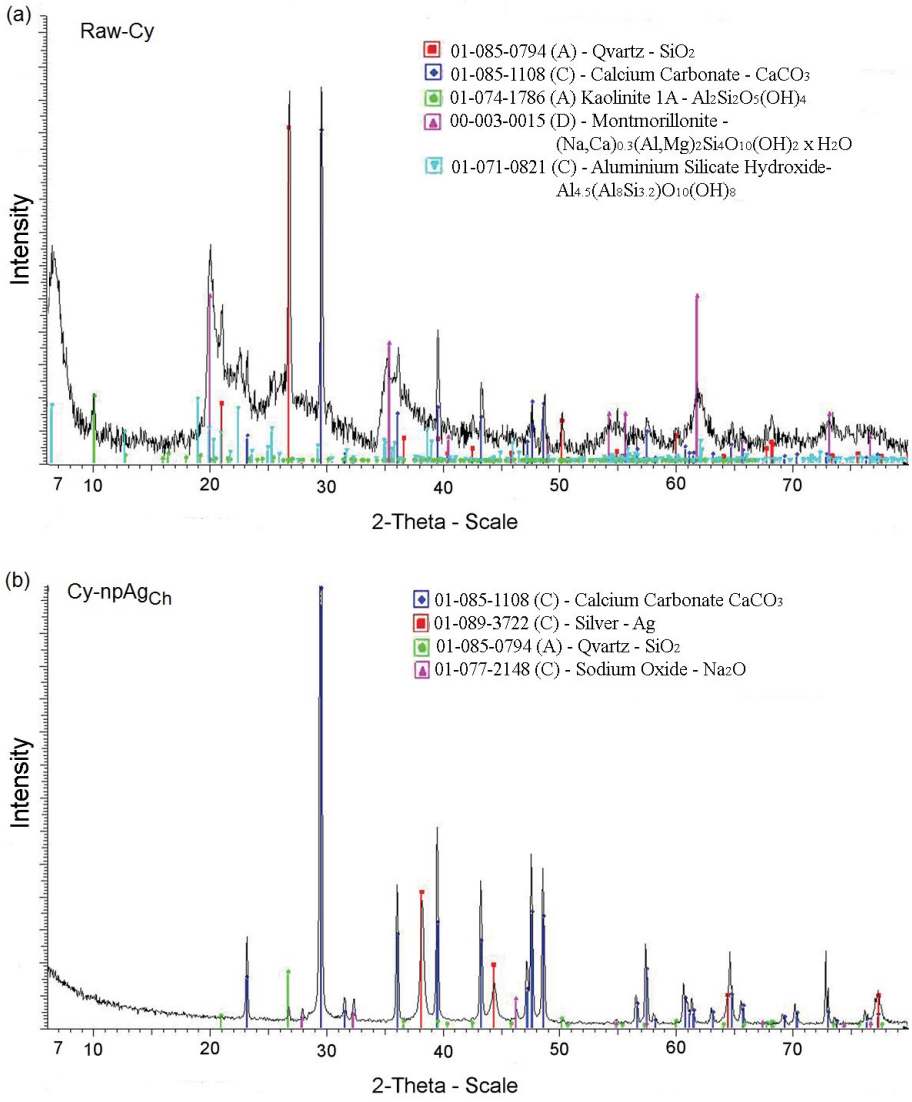

Fig. 2. XRD pattern of (a) raw-Cy and (b) Cy-npAg$_{Ch}$ adsorbents.

3.7.1. Adsorption kinetics

To study the adsorption kinetics, the pseudo-first, pseudo-second-order (PSO) and second-order kinetic models were used [5,13,33,40,41]. In a preliminary adsorption study due to lower determined PSO rate constants, that is, 15%–20% lower for raw-Cy. Kinetic study of diazinon removal in a dark and ambient condition (irradiation under the influence of sunlight) was performed to distinguish the contribution of adsorption and photodegradation processes to overall pollutant removal. In a further step, a detail kinetic study was performed and, additionally, the rate controlling step of adsorption was evaluated using Weber–Morris model (W–M) [48]. The used kinetic model equations are given in Table S4. The complex nature of the process of overall metal ions uptake was considered either by one general step, as it was described by PSO equation [Table S4; Eq. (S4)], or it could be analyzed as a consecutive/competitive process. Generally, in adsorption process four consecutive steps could be operative: the first one presents diffusion in a bulk, second describes diffusion across the liquid film to the adsorbent surface (surface diffusion), the third represents transport of adsorbate in the pores and/or along the pore walls (intra-particle diffusion), and last, fourth step is adsorption/desorption between adsorbate and active sites. The W–M fitting revealed that two successive linear steps describe the adsorption process: fast kinetics in the first step and slower in the second part. Overall ion transport was mainly controlled by intra-particle diffusion as indicated by a large value of intercept, that is, constant *C* (Table 4). The first linear part describes external mass transfer to the adsorbent surface, while the second part describes the processes which take place in a porous structure of adsorbent, and strongly related to pore geometry and network density of Cy-npAg$_{Ch}$. The intra-particle and film diffusion resistance slows down adsorbate transport, that is, net transport in the direction of the variable time-dependent concentration gradient. At the final stage of the process, the adsorption takes place at a low rate until saturation

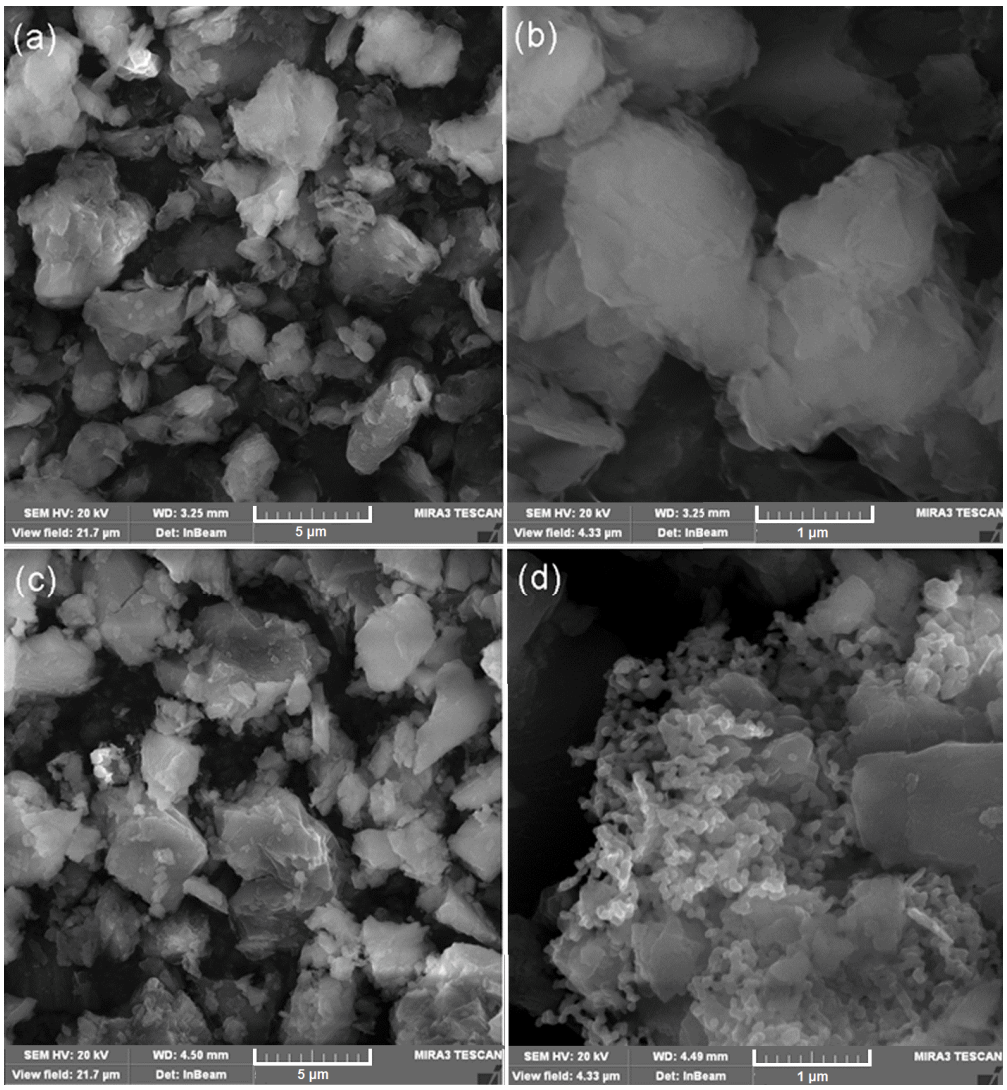

Fig. 3. SEM images of raw-Cy (a and b) and Cy-npAg$_{Ch}$ (c and d) adsorbent.

Table 3
Kinetic parameters for adsorption Cd^{2+} and Ni^{2+} ion and diazinon onto Cy-npAg$_{Ch}$ ($C_{i\left[Cd^{2+}\text{and } Ni^{2+}\right]}$ = 5.00 mg L^{-1}; $C_{i[\text{Diazinon}]}$ = 30.00 mg L^{-1}; m/V = 2 g dm^{-3}, pH = 6.5; T = 298°K)

Kinetic models	Parameters	Cd^{2+}	Ni^{2+}	Diazinon*
Pseudo-first	q_e (mg g^{-1})	35.693	31.721	26.288
	k (k_1, k_2)	0.0598	0.0423	0.0302
	R^2	0.945	0.926	0.882
Pseudo-second	q_e (mg g^{-1})	39.930	30.01	48.290
	k (k_1, k_2)	0.00127	0.0007	0.00145
	R^2	0.991	0.953	0.992
Second-order	q_e (mg g^{-1})	39.930	30.013	48.290
	k (k_1, k_2)	0.0703	0.0661	0.00225
	R^2	0.967	0.864	0.934

*Overall rate constant of diazinon removal including both adsorption and photodegradation. PSO constants for pure adsorption was evaluated to be ~13.2% lower (based on experiments performed in dark).

of all available surface sites is achieved [13,14]. Also, the Dunwald–Wagner model (D–W) and homogenous solid diffusion model (HSDM) were used for the determination of diffusional properties of studied ions and diazinon.

Results of D–W and HSDM modeling is not of high statistical quality. Applicability of PSO equations with respect to D–W and HSDM models lye in the fact that the former one is defined without any constrains and limitation of process conditions. In the other hand, couple assumptions considered in the course of definition of HSDM model: surface diffusion is a process of adsorbate transport inside the pore (the adsorbent is a homogeneous sphere), the rate-controlling process is affected by film and surface diffusion, a driving potential is determined by mass transfer resistance in a liquid film of the adsorbent outer surface, and fast equilibration at outer surface is established [49]. D–W was used for the description of the processes based on the Fick's second law for diffusion into or out of a sphere. According to the results from Table 4, describes the fast adsorption rate in the first step and a significant decrease in diffusional transport in second. Correlation line does not cross the origin

Table 4
W–M kinetic parameters for adsorption Cd^{2+} and Ni^{2+} ion and diazinon onto Cy-npAg$_{Ch}$ ($C_{i\left[Cd^{2+}\text{and } Ni^{2+}\right]}$ = 5.00 mg L^{-1}; $C_{i[Diazinon]}$ = 30.00 mg L^{-1}; pH = 6.5; T = 298°K)

Kinetic model		Constants	Cd^{2+}	Ni^{2+}	Diazinon***
D–W		K (min^{-1})	0.0154	0.00743	0.01425
		R^2	0.903	0.934	0.845
HSDM		Ds (m^2 s^{-1})	2.02E–11	1.18E–11	1.77E–11
		R^2	0.899	0.965	0.828
W–M	Step 1*	k_{p1} (mg g^{-1} min$^{-0.5}$)	4.417	1.936	5.927
		C (mg g^{-1})	0.040	0.046	0.605
		R^2	0.992	0.999	0.995
	Step 2**	k_{p2} (mg g^{-1} min$^{-0.5}$)	0.307	0.320	0.606
		C (mg g^{-1})	29.204	17.15	35.027
		R^2	0.999	0.992	0.994

*Intra-particle diffusion; **Equilibrium; ***Overall rate constant of diazinon removal including both adsorption and photodegradation.

and small value indicates that intra-particle diffusion is the main diffusional process which determines overall adsorbate transport. The obtained results are in accordance with the textural properties of Cy-npAg$_{Ch}$. In regard to defined model limitation and results of HSDM kinetic data correlation, it is clear that surface diffusion is not rate limiting process, but participation of both intra-particular (main) and surface (minor participation) diffusion determines overall kinetic of the process.

3.7.2. Activation energy of the adsorption

According to the results of kinetic study performed at three temperatures, that is, 298°K, 308°K, and 318°K, it was possible to calculate activation energy according to Arrhenius equation [Eqs. (S9) and (S10)] giving a plot describing the dependence of ln$k$ vs T^{-1} according to the results given in Table S5. The calculated activation energy is as follows, E_a = 6.59, 7.35, and 14.48 kJ mol^{-1} for Cd^{2+}, Ni^{2+} ion, and diazinon, respectively. The small differences between the two activation energies point to the similar mechanism of metal ions binding onto the adsorbent. Magnitudes of the activation energy may help in understanding the mechanism of the adsorption in studied system. Physisorption or physical adsorption generally possesses activation energy bellow 40 kJ mol^{-1}, while the chemisorption requires more energy and activation energy is higher than 40 kJ mol^{-1} [50]. Obtained results indicate that physisorption is a dominant process in the removal of both Cd^{2+} and Ni^{2+} and diazinon as well. In practice, both physisorption and chemisorption could be operative simultaneously; for instance, the molecule layer can be physically adsorbed as the outer layer on the chemisorbed layer at the adsorbent surface [51].

3.7.3. Study of the competing ions influence on the adsorption process

The kinetic study under competitive conditions gives valuable results on the evaluation of affinity/selectivity for pollutants of interest. Obtained results offer necessary input parameters, that is, dominate variable and modeling parameters, for the design of adsorbent capacity for selective pollutant removal from natural/polluted water. Results of competitive adsorption of Cd^{2+} and Ni^{2+} ion and diazinon in the presence of single interfering ion: Pb^{2+}, As(V), and Fe^{3+} and multicomponent system [Pb^{2+}/As(V)/Fe^{3+}], modeled using PSO equation, are given in Table 5.

Single competitive Cd^{2+} removal (Table 5) shows the highest influence of the system of three cations (Pb^{2+}/As^{5+}/Fe^{3+}; 44% lower k_2), followed by Pb^{2+} (35%), Fe^{3+} (15%), and As(V) (18%). Similar trend of 51%, 44%, 16%, and 19% of k_2 decrease, respectively, is obtained for Ni^{2+}. Similar trend of the adsorption capacity decrease was observed for both cations. Obtained results indicate larger influences of cation, while oxyanion showed low influences at pH > pH$_{PZC}$. It was published that npAg incorporated in carbonized yeast cells showed low capacity for As(V) removal (0.975 mg g^{-1}) [52]. The highest decrease of diazinon removal was obtained in the presence of Pb^{2+} (32%), and generally, more effective interactions were established between Cy-npAg$_{Ch}$ and cations. Kinetic study of diazinon removal performed in a dark showed that appropriate catalytic influences of iron(III) ion on photodegradation efficiency. Obtained results indicate low selectivity with respect to both cations and anions, which means that Cy-npAg could be effectively used as a general-purpose adsorbent for preferential cations with simultaneous anion removal from the multicomponent system. Interfering effects of studied ions on the efficiency of diazinon removal is highly detrimental, and design of the technology for diazinon removal in natural water.

3.8. Adsorption study

The experimental data were compared to the models of the Langmuir, Freundlich, Temkin, and Dubinin–Radushkevich isotherms utilized elsewhere in previous research within the literature [2,33,53,54]. More data on the used isothermal models are given in the Supplementary material [Table S6, Eqs. (S11)–(S14)]. The results from adsorption study are given in Table 6. Analysis of the experimental data of diazinon and Cd^{2+}, Ni^{2+} ion adsorption on the Cy-npAg$_{Ch}$ indicate that the best fit of the adsorption data was obtained using Freundlich isotherm model for diazinon and ions Ni^{2+} and Dubinin–Radushkevich isothermal model for Cd^{2+} ions (Fig. S7).

Highest value of adsorption capacity was obtained for diazinon (65.94 mg g^{-1}), somewhat lower for Cd^{2+} (57.78 mg

Table 5
Results of the competitive Cd^{2+} and Pb^{2+} ion and diazinon removal onto Cy-npAg$_{Ch}$ in the presence of interfering ions ($C_{i[Cd^{2+}\text{and } Ni^{2+}]}$ = 5.00 mg L^{-1}; $C_{i[\text{Diazinon}]}$ = 30.00 mg L^{-1}; pH 6.5)

Adsorbate	Parameters	Non-competitive condition	Competitive conditions			
			Pb^{2+}*	As(V)*	Fe^{3+}*	Pb^{2+}/As(V)/Fe^{3+}**
Cd^{2+}	q_e (mg g^{-1})	39.93	25.651	36.156	33.762	21.235
	$k_2 \times 10^3$	0.00127	0.00083	0.00114	0.00108	0.00071
	R^2	0.991	0.994	0.996	0.995	0.988
Ni^{2+}	q_e (mg g^{-1})	30.01	14.462	24.854	22.665	11.528
	k_2	0.0007	0.00034	0.00059	0.00054	0.00031
	R^2	0.953	0.987	0.991	0.985	0.981
Diazinon***	q_e (mg g^{-1})	48.290	15.242	20.863	18.846	10.335
	k_2	0.00145	0.00045	0.00066	0.00058	0.00034
	R^2	0.992	0.985	0.978	0.991	0.982

*Single competitive condition ($C_{i[Fe^{3+}]}$ = 1.06 mg L^{-1}; $C_{i[As(V)]}$ = 0.98 mg L^{-1}; $C_{i[Fe^{3+}]}$ = 1.22 mg L^{-1}); **System of three anion used altogether as in single competitive condition; ***overall rate constant of diazinon removal including adsorption and photodegradation. PSO adsorption constants in a competitive condition were 14.8%, 18.1%, and 24.6% lower in presence of Pb^{2+}, As(V), and Fe^{3+}, respectively (based on the experiments performed in dark).

	Pb^{2+}***	As(V) ***	Fe^{3+}***	Pb^{2+}/As(V)/Fe^{3+}***
q_e (mg g^{-1})	12.988	17.084	14.206	6.866
k_2	0.000403	0.00053	0.000435	0.000251
R^2	0.986	0.979	0.920	0.901

*** The values in dark

g^{-1}), and lowest for Ni^{2+} (33.93 mg g^{-1}) at 25°C. This unusual result, except higher C_i for diazinon, could be explained by higher affinity of specific electronic density of diazinon, defined by MEP surface (Fig. S4), to Cy-npAg$_{Ch}$ surface. Among many factors, structural/spatial arrangement of studied molecule play a significant role, and thus optimization of geometry was performed using PM6 method incorporated in MOPAC program package. Both factor, coincidental approach (orientation) and type of bonding of diazinon, is largely influenced by optimal geometry and electrostatic potential of diazinon (MEP surface; Fig. S4), as well as actual surface charges of the adsorbent. Visualization of MEP surface of diazinon defines possible sites which could participate in an interaction with adsorbent functionalities/charges. MEP surface indicates that the most dominant structure with negative charges could be pyrimidine ring and thiophosphate group (Fig. S4). At operative pH 6, which is slightly higher than pH_{PZC}, it could be expected that the positive MEP surface of diazinon establishes higher intensity interactions with negative adsorbent sites/functionalities. Due to inhomogeneous surface coverage of raw-Cy with npAg additional contribution to increased diazinon adsorption was attributed to specific interactions between the exchangeable clay cations and the P = S group [55]. Some structural features of diazinon such as the presence of thiol tautomeric form (tautomeric equilibrium shifted to thiol as energetically favorable type of bonding with Cy-npAg$_{Ch}$) could be beneficial structure able to establish effective interaction at the organic-metal interface. It was shown that mostly negatively charged thiol group creates desirable molecular interactions at the surface of npAgs [55,56], and intermolecular distance between adsorbed molecules should be large enough to minimize repulsive interactions. In general, a variety of different interactions could be formed at different contributions to overall adsorption process. Thus, diazinon adsorption highly depends on both npAg and neat raw-Cy surface properties, which are able to participate in a different ionic/electrostatic, covalent, and ion-exchange interactions. The key of the future study to understand the bonding type at heterogeneous Cy-npAg$_{Ch}$ and similar surface will relate to characterization of interfacial density distribution using instrumental analysis and ab-inito theoretical calculation. Many parameters should be included: symmetry rules and character of orbital participating in the bonding, the coordination degree, geometry and strength of the bond, structure/orientation of the attached moieties, and structural feature, etc., to obtain clear picture on the mechanism of adsorption.

The adsorption energy, obtained from the Dubinin–Radushkevich isotherm, maybe a reliable indicator of the adsorption mechanism. If the value E is below 8 kJ mol^{-1}, the adsorption process can be considered to be physical adsorption. In contrast, if the value of E is in the range of 8–16 kJ mol^{-1}, it is chemical adsorption. Table 6 notes that the E value in the range indicating physical adsorption in diazinon and chemical adsorption in the investigated metal ions [57].

The calculation of separation factor (R_L; Eq. S15) points to the feasibility of adsorption process: irreversible (R_L = 0), favorable (0 < R_L < 1), linear (R_L = 1), and unfavorable (R_L > 1). R_L for the adsorption of diazinon, Cd^{2+}, and Ni^{2+} on Cy-npAg$_{Ch}$ is in the range from 0.172 to 0.573, 0.0013 to 0.024, and 0.0011 to 0.114, respectively, indicating the adsorption of Cd^{2+} and Ni^{2+} ions and diazinon on Cy-npAg$_{Ch}$ is favorable. Additionally, comparative adsorption study of diazinon, Cd^{2+}, and Ni^{2+} removal by using Cy-npAg$_{Ch}$ and raw-Cy adsorbents showed the significant decrease of q_e: 74.26 vs. 46.27 mg g^{-1} for diazinon, 62.32 vs. 49.38 mg g^{-1} for Cd^{2+}, and 35.9 vs. 29.73 mg g^{-1} for Ni^{2+}, respectively. These results clearly show the significance of modification of raw-Cy to the improvement of adsorption performance of Cy-npAg$_{Ch}$.

Table 6
Adsorption isotherm parameters for Cd^{2+}, Ni^{2+}, and diazinon adsorption on the Cy-npAg$_{Ch}$ ($C_{i[Cd^{2+}\text{and } Ni^{2+}]}$ = 5.00 mg L^{-1}; $C_{i[Diazinon]}$ = 30.00 mg L^{-1}; t = 90 min; pH = 6.5)

Isotherm model	Model parameters	Cd^{2+}			Ni^{2+}			Diazinon*		
Temperature		25°C	35°C	45°C	25°C	35°C	45°C	25°C	35°C	45°C
Langmuir	q_m (mg g^{-1})	57.78	60.09	62.32	33.93	34.70	35.49	65.94	70.65	74.26
	K_L (L mol^{-1})	73,00,604	86,67,164	11,368,136	58,96,356	60,43,811	62,85,831	4,53,466.6	4,89,074.4	5,25,290.8
	K_L (L mg^{-1})	64.952	77.11	101.14	100.449	102.961	107.084	1.49	1.607	1.726
	R^2	0.988	0.987	0.981	0.946	0.962	0.975	0.851	0.861	0.867
Freundlich	K_F (mg g^{-1}) (dm^3 mg^{-1})$^{1/n}$	54.33	56.71	58.21	34.07	34.65	35.280	42.071	44.44	47.87
	$1/n$	0.1	0.1	0.099	0.099	0.099	0.099	0.166	0.172	0.167
	R^2	0.823	0.812	0.804	0.999	0.999	0.999	0.991	0.998	0.993
Temkin	A_T (dm^3 g^{-1})	1,67,764	1,81,545	2,55,060	4,71,706	4,50,592	4,58,055	109.47	88.156	110.41
	B_T	4.575	4.751	4.828	2.573	2.640	2.694	8.816	9.764	10.08
	b (J mol^{-1})	336.31	333.12	341.04	673.64	640.34	609.99	281.17	262.38	262.37
	R^2	0.947	0.951	0.950	0.913	0.903	0.891	0.978	0.995	0.996
Dubinin–Radushkevich	q_m (mg g^{-1})	57.76	60.69	63.62	32.91	34.30	35.79	59.88	63.63	66.90
	K_{ad} (mol^2 KJ^{-2})	7.57	7.52	7.48	7.49	7.45	7.40	8.53	8.47	8.42
	E (KJ mol^{-1})	8.125	8.152	8.177	8.172	8.194	8.218	7.654	7.681	7.704
	R^2	0.994	0.995	0.994	0.990	0.994	0.996	0.737	0.760	0.753

*Overall adsorption capacity of diazinon removal. The q_m were lower for 9.6%, 11.4%, and 12.2% for experiments performed at 25°C, 35°C, and 45°C, respectively (based on experiments performed in dark).

3.8.1. Adsorption thermodynamic

The thermodynamic parameters, calculated according to Eqs. (S16) and (S17), also indicated on adsorption mechanisms. The negative $\Delta G°$ values (Table 7) specify that adsorption of Cd^{2+}, Ni^{2+}, and diazinon on Cy-npAg$_{Ch}$ is a spontaneous process. Since the $\Delta G°$ decreases with a temperature increase, the process is indicated to be more efficient at higher temperatures. Generally, the change of free energy in the case of physisorption is between –20 and 0 kJ mol^{-1}, for both physisorption and chemisorption it is between –20 and –80 kJ mol^{-1}. It means that adsorption of Cd^{2+}, Ni^{2+}, and diazinon on Cy-npAg$_{Ch}$ is a process with an appropriate contribution of both physisorption and chemisorption processes.

The positive values of $\Delta H°$ indicate that the adsorption of Cd^{2+}, Ni^{2+}, and diazinon on Cy-npAg$_{Ch}$ is an endothermic process. The low enthalpy values of $\Delta H° < 20$ kJ/mol confirms the physisorption process for the removal of diazinon, Cd^{2+}, and Ni^{2+} ions, on the adsorbent [28]. The positive entropy change values $\Delta S°$ (Table 7) indicate an increase in boundary solid-liquid surface disorder due to numerous energetically different intermolecular interactions, which are mostly electrostatic in nature. The cation adsorption contributes to the entropy decrease, while ions release from the adsorbent surface causes increasing of the system's entropy. The highest value of $\Delta S°$ found for Cd^{2+} could be explained by the higher value of ionic radii and thus different packing/interaction in a multi-layered structure at the adsorbent surface.

3.8.2. Effect of interfering ions

Study of the influences of interfering ions, usually present in natural water, give realistic information on the potential applicability of synthesized adsorbent. Affinity/selectivity could be estimated from the competitive study and could give information about successfulness of the removal of ions of interest in the presence of ions commonly found in natural water. Adsorption experiments were performed with model water spiked with 100 μg L^{-1} of the selected pollutants. Adsorption results obtained under competitive conditions are given in Tables 8 and 9.

The detrimental effect of the common interfering ions on the adsorption efficiency of Cd^{2+} and Ni^{2+} showed similar behavior with the most significant influence of Pb^{2+} ion. Otherwise low interference of competitive anions/oxyanions was found, which means higher affinity of a negatively charged adsorbent surface to positively charged cations at $pH > pH_{PZC}$. Competitive study of the anions/cations removal from real water samples showed low selectivity of Cy-npAg for ions present in real water. Removal efficiency depends on valence state of cations, as well as actual concentration. Higher affinity of trivalent ions, that is, Al^{3+} and Fe^{3+}, for Cy-npAg$_{Ch}$ is defined in competitive adsorption study at an equal concentration of ions: two- to three-fold higher cations uptake is found with respect to Ni^{2+} while somewhat lower, that is, nearly two times, is found with respect to Cd^{2+}. Also, results of adsorption study using real water sample showed satisfactory efficiency of pollutant removal with low selectivity (Table S7). Obtained results showed good capacity and adsorption kinetics with low selectivity of Cy-npAg$_{Ch}$ adsorbent, which means its useful applicability as general purpose adsorbent used in water purification processes.

3.9. Desorption study

The regeneration of the adsorbent could provide long term usability in a consecutive adsorption/desorption cycles. In general, two main goals should be achieved by

Table 7
Calculated Gibbs free energy of adsorption, enthalpy and entropy for Cd^{2+}, Ni^{2+}, and diazinon adsorption on Cy-npAg$_{Ch}$ at 298°K, 308°K, and 318°K

Adsorbate	$\Delta G°$/kJ mol^{-1}			$\Delta H°$/kJ mol^{-1}	$\Delta S°$/J mol^{-1} K^{-1}	R^2
T (K)	298	308	318			
Cd^{2+}	–49.13	–51.22	–53.60	17.41	223.04	0.978
Ni^{2+}	–48.60	–50.29	–52.03	2.52	171.42	0.977
Diazinon	–42.24	–43.85	–45.46	5.80	161.12	0.999

Table 8
Efficiency of pollutant removal by Cy-npAg$_{Ch}$ in the presence of interfering anion

System	pH$_i$	Ion*/% removal	Content of the interfering anions (mg L^{-1})					
			$Cr_2O_7^{2-}$	Cl^-	SO_4^{2-}	F^-	NO_3^-	PO_4^{3-}
Model water**	6.4		0.3	6.5	22.8	0.10	4.5	19.4
	6.3	Cd^{2+}/97	BDL***	6.2	21.2	0.10	4.2	18.1
Cy-npAg$_{Ch}$/model water	6.3	Ni^{2+}/94	BDL	6.1	18.9	0.10	4.1	18.0
	6.3	Diazinon/84	BDL	6.4	22.0	0.10	4.4	19.1

*Percent of pollutant removal (mean value from three determination); **anion content in water spiked with 100 μg L^{-1} of pollutant without adsorbent; ***BDL, below detection limit.

Table 9
Efficiency of pollutant removal by Cy-npAg$_{Ch}$ in the presence of interfering cation

System	pH$_i$	Ion*/% removal	Content of the cations (μg L^{-1})**					
			Cu^{2+}	Ni^{2+}	Zn^{2+}	Cd^{2+}	Pb^{2+}	Si
Model water**	6.4		32	15	445	22	39.2	1,556
Cy-npAg$_{Ch}$/model water	6.2	Cd^{2+}/91	22	8	362	11***	4.4	1,226
	6.2	Ni^{2+}/90	20	19***	371	BDL	3.1	1,132
	6.2	Diazinon/77	12	13	422	BDL	BDL	1,446

*Percent of pollutant removal (mean value from three determination); **Cation content in water spiked with 100 μg L^{-1} of the pollutant of interest; ***Spiked with 100 μg L^{-1}.

designing new adsorbent: high adsorption performance (capacity/adsorption, rate/affinity, etc.) and desorption efficiency which contributes to the lower adsorbent's total cost. According to the calculated R_L, which is close to zero (from 0.0013 to 0.024 and 0.0011 to 0.114) it is expected that adsorption shows significant levels of irreversibility. In order to check this assumption, different desorption agents, such as NaOH, citric acid, ethylenediaminetetraacetic acid (EDTA), conc. hydrochloric acid (HCl), phosphoric acid, and oxalic acid were used. Strong bases and acids are commonly used to elute cations. Desorption efficiency represents the percentage of the amount of heavy metal desorbed to the amount of heavy metal adsorbed per mass unit of the adsorbent. As an example, the pH dependent desorption of Ni^{2+} and Cd^{2+} ions with citric acid are provided in Fig. 4. It is found that desorption of both ions increases with the pH values decrease. Desorption of Ni^{2+} ions sharply decreased at pH > 5. Acceptable desorption at pH 5: 78% for Ni^{2+} and 86% for Cd^{2+} was found. Similar behavior was obtained by using EDTA, oxalic, and citric acid. By using HCl acceptable desorption was achieved at pH < 3 which is not acceptable from the point of post-treatment of eluent solution contributing to an increase in technology cost. The most efficient desorption agents were found to be citric (91%) and oxalic (87%) at pH 5.

Desorption results indicate that Cy-npAg$_{Ch}$ may be utilized consecutively for the removal of heavy metals from water in five consecutive cycles where the removal efficiency decreases to 64% for Cd^{2+} and 55% for Ni^{2+} by using citric acid. Application of npAg and silver ion based materials in water purification and disinfection is closely related to couple criteria: activity, reusability, stability, and side-effects such as destruction products and ion release in water flow. Consideration of potential application should include a critical consideration of maximum contamination levels of residuals prescribed by regulation. Silver levels in drinking water not treated with silver ion as disinfectant usually vary between "non-detectable" and 5 μg L^{-1}, that is, 5 ppb. Water treated with silver ions may have levels of 50 μg L^{-1} or even higher, and mainly silver ions is present as non-dissociated silver chloride [7,58].

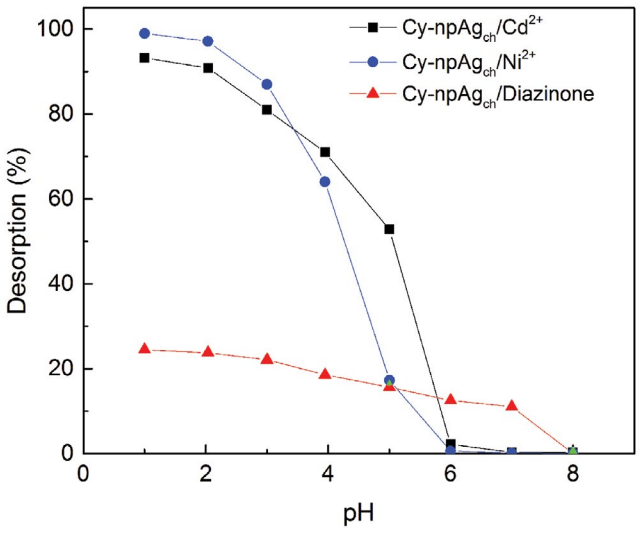

Fig. 4. Desorption of Cd^{2+} and Ni^{2+} from Cy-npAg$_{Ch}$ at varying pH (desorption agent citric acid).

3.10. Antimicrobial activity

Standard disinfection methods, for example, chlorination and ozonation, are usually applied as an unavoidable step in a water purification technology where is necessary to remove/control microbial pathogens. These general disinfection technologies showed high effectiveness, due to strong oxidative capability and reactivity of chemical which could produce intermediary products in a reaction with natural organic matter. Oxidative and chlorinated by-products, that is, disinfection byproducts (DBP), could show diversity of biological activities, and some of them are identified as carcinogenic [59]. In accordance to that, significant effort was devoted to the development of new disinfection technology/disinfectants with minimum/low level of DBP production in the course of technology implementation. Development of silver based disinfectant in the form of npAg, and immobilized on different support would offer many advantageous over existing material. Among many possible applications of silver based disinfectants, their antimicrobial potential found widespread use in modern human life: biomedical, industry, and environmental protection [60–62]. Many factors influence the magnitude of npAg antimicrobial activity: leaching of silver species, size, and shape of npAg, environment to be applied, surface charge/properties, and surface modification/coating. The antimicrobial properties of silver based disinfectants originate from either release of Ag$^+$ ion which cause disruption of bacterial membrane and/or, generation of reactive oxygen species (ROS) [61,62].

It was defined close relation of the size-dependent activity of npAg with respect to ROS species formation [63]. Also, the most intriguing question on toxicity of the released Ag^+ ion was undoubtedly resolved, and lack of toxicity of npAg synthesized in anaerobic conditions was also proved [64]. According to this finding applied condition for Cy-npAg$_{Ch}$ synthesis provide a reductive environment with minimum oxidized Ag, and thus low toxicity of this material would be expected.

To better understand material properties about synthesis method, both Cy-npAg$_{Ch}$ and Cy-npAg$_{Ph}$ were used in an antimicrobial study, and results was compared with the material obtained by impregnation of raw-Cy with Ag^+ ion, that is, Cy-Ag^+. Detail on the applied method is given in Supplementary material. After incubation at 37°C for 24 h with shaking at 180 rpm, bacterial growth was assessed by measuring the absorbance. Inhibition of bacterial growth was expressed as a percentage of growth without any material, which was set to be 100%. The npAgs in Cy-npAg$_{Ch}$ exhibited good antimicrobial activities with inhibition zones in the range of 13–20 mm. The npAg on Cy-npAg$_{Ch}$ against Gram-positive bacteria (*S. aureus*) and Gram-negative bacteria (*E. coli* and *P. aeruginosa*) of 64%, 39%, and 70% antibacterial colony growth reduction, respectively [62]. Selected results are presented as a histogram in Fig. 5.

Significantly better antimicrobial activity was obtained using Cy-Ag^+ material, and somewhat better for Cy-npAg$_{Ph}$ giving nearly 95%–97% and 62%–82% colony growth reduction, respectively. These results offer a beneficial opportunity to use Cy-Ag^+ as effective antibacterial material, while its adsorptive characteristic (~8% lower q_m) is comparative to Cy-npAg$_{Ch}$. However, such results are valid only for the first

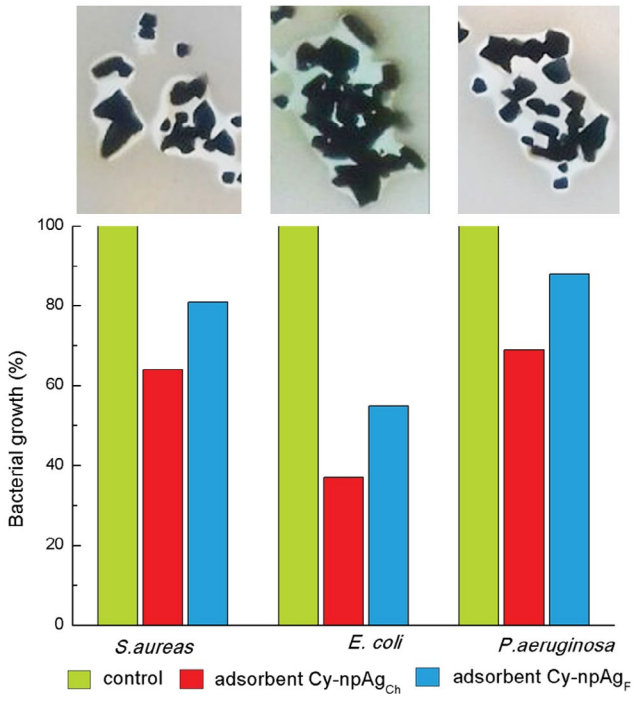

Fig. 5. Histogram of the antimicrobial activity of the Cy-npAg$_{Ch}$ adsorbent.

adsorption cycle, and, in a subsequent cycle activity decrease for more than 60%, and, in third cycle showed no activity as it was found for unmodified raw-Cy. High antibacterial activity of Cy-Ag^+ originates from the release of a significant amount of loosely bonded Ag^+. Thus the leaching potential of synthesized material to release disinfecting species, that is, silver ion, was also investigated. Leaching test of Cy-Ag^+ showed >2.5 ppm of Ag^+ which exceeded prescribed maximum allowable concentration WHO Guideline = 0.1 mg/L [65], and thus it could exert high negative environmental impact in a real application. The Cy-npAg$_{Ph}$ shows similar behavior in the second cycle adsorption capacity decreases for ~25% and the antibacterial effect decrease for 32% were obtained, respectively. Intermediary properties show Cy-npAg$_{Ch}$, that is, lower antimicrobial and somewhat higher adsorptive properties than Ag^+/Cy, while multi-cycle applicability is notably improved with respect to both properties. Regardless to the lower antibacterial activity of Cy-npAg$_{Ch}$, with respect to both Cy-Ag^+ and Cy-npAg$_{Ph}$, its applicative potential is higher due to the longer possible exploitation period in relation to both adsorptive and antibacterial properties. In general, the low release of Ag^+ in presence of Cy-npAg$_{Ch}$ (<0.1 mg dm^{-3}) indicates acceptable toxicity in accordance to guideline prescribed by WHO. Thus, the synergetic effect of both effect npAg structure/properties (main) and Ag^+ generation (lower) could be contributing factors to observed antibacterial activity [66,67], which is in line with fact that the larger the surface area the higher antibacterial activity is a consequence.

4. Conclusions

The presented results demonstrated that montmorillonite clay, raw-Cy, and one modified with npAgs, Cy-npAg$_{Ch}$, may be used as an effective adsorbent for the removal of diazinon and Cd^{2+} and Ni^{2+} ions from water. The best adsorption performances of Cy-npAg$_{Ch}$ was obtained by controllable reduction of silver ion onto raw-Cy to provide 4.8 wt.% of npAg deposit. The precipitation of the optimal quantity/structure of npAg impregnated clay was achieved by performing multi-step precipitation. The use of RSM for the design of adsorption experiments was aimed to reduce the expensive and time-consuming experimental work and analysis, as well as to test the possibility to predict adsorption data based on a limited number of experimentally obtained ones.

The best fitting of adsorption data was obtained using the Langmuir and Dubinin–Radushkevich isotherm models, while the kinetic data followed the PSO model. The thermodynamic studies also indicate that the reaction was endothermic in nature, as well as that the physisorption and chemisorption adsorption mechanism are operative in a processes of Ni^{2+} removal, while physisorption dominates in a process of Cd^{2+} removal. The time-dependent adsorption data, fitted using W–M model, predicted intra-particle diffusion as a main rate-controlling step with a minor contribution of surface diffusion. The desorption study confirmed that Cy-npAg$_{Ch}$ could be consecutively used in processes of cation removal/regeneration in five cycles. Loaded samples were found to have significant activity against examined microorganisms, although they were found less active than

standard drugs. In summary, the presented results indicate that Cy-npAg_{Ch} offers the most valuable choice to obtain both satisfactory adsorption performance and reusability, and disinfection efficacy for longer life-time exploitation antimicrobial activity (>80% in the fifth cycle).

Acknowledgment

The authors acknowledge the financial support from the Ministry of Education, Science and Technological Developments of the Republic of Serbia, Projects No. III45019 and OI172057.

References

[1] Z.J. Bajić, Z.S. Veličković, V.R. Djokić, A.A. Perić-Grujić, O. Ersen, P.S. Uskoković, A.D. Marinković, Adsorption study of arsenic removal by novel hybrid copper impregnated tufa adsorbents in a batch system, Clean – Soil Air Water, 44 (2016) 1–12.
[2] Z.S. Veličković, N. Ivanković, V. Striković, R. Karkalić, D. Jovanović, Z. Bajić, J. Bogdanov, Investigation of soil properties influence on the heavy metals sorption by plants and possibilities for prediction of their bioaccumulation by response surface methodology, J. Serb. Chem. Soc., 81 (2016) 947–958.
[3] M.K. Uddin, A review on the adsorption of heavy metals by clay minerals, with special focus on the past decade, Chem. Eng. J., 308 (2017) 438–462.
[4] S.S. Gupta, K.G. Bhattacharyya, Immobilization of Pb(II), Cd(II) and Ni(II) ions on kaolinite and montmorillonite surfaces from aqueous medium, J. Environ. Manage., 87 (2008) 46–58.
[5] H. Liu, X. Cai, Y. Wang, J. Chen, Adsorption mechanism-based screening of cyclodextrin polymers for adsorption and separation of pesticides from water, Water Res., 45 (2011) 3499–3511.
[6] M. Rivera-Garza, M.T. Olguõn, I. Garcõa-Sosa, D. Alcantara, G. Rodrõguez-Fuentes, Silver supported on natural Mexican zeolite as an antibacterial material, Microporous Mesoporous Mater., 39 (2000) 431–444.
[7] WHO, Guidelines for Drinking-water Quality, First addendum to 3rd ed., Vol. 1, Geneva, World Health Organization, 2006.
[8] X. Wu, An ion adsorption model related to the change in the standard chemical potential of adsorption reactions, Adsorpt. Sci. Technol., 29 (2011) 747–768.
[9] M. Castro, A. Martinez, A. Gil-Villegas, Modelling adsorption isotherms of binary mixtures of carbon dioxide, methane and nitrogen, Adsorpt. Sci. Technol., 29 (2011) 59–70.
[10] Z.J. Bajić, V.R. Djokić, Z.S. Veličković, M.M. Vuruna, M.Đ. Ristić, N.B. Issa, A.D. Marinković, Equilibrium, kinetic and thermodynamic studies on removal of Cd(II), Pb(II) and As(V) from wastewater using Carp (*Cyprinus Carpio*) scales, Dig. J. Nanomater. Bios., 8 (2013) 1581–1590.
[11] S.K. Myasnikov, A.Y. Tikhonovu, A.P. Chipryakova, N.N. Kulov, Removal of heavy metal ions from water by a combined sorption–crystallization process using activated clays, Theor. Found. Chem. Eng., 50 (2016) 366–382.
[12] L. Ma, Q. Chen, J. Zhu, Y. Xi, H. He, R. Zhu, Q. Tao, G.A. Ayoko, Adsorption of phenol and Cu(II) onto cationic and zwitterionic surfactant modified montmorillonite in single and binary systems, Chem. Eng. J., 283 (2016) 880–888.
[13] R. Srinivasan, Advances in application of natural clay and its composites in removal of biological, organic, and inorganic contaminants from drinking water, Adv. Mater. Sci. Eng., 2011 (2011) 1–17, doi.org/10.1155/2011/872531.
[14] K. Taik-Nam, J. Choong, Adsorption characteristics of sericite for nickel ions from industrial waste water, J. Ind. Eng. Chem., 19 (2013) 68–72.
[15] J.P. Kumar, P.V.R.K. Ramacharyulu, G.K. Prasad, B. Singh, Montmorillonites supported with metal oxide nanoparticles for decontamination of sulfur mustard, Appl. Clay Sci., 116–117 (2015) 263–272.
[16] A. Bée, L. Obeid, R. Mbolantenaina, M. Welschbillig, D. Talbot, Magnetic chitosan/clay beads: a magsorbent for the removal of cationic dye from water, J. Magn. Magn. Mater., 421 (2017) 59–64.
[17] C.A.L. Junior, D.S.A. Silva, A.P.C. Filho, E.F. Lucasc, S.A.A. Santana, Smectite clay modified with quaternary ammonium as oil remover, J. Braz. Chem. Soc., 28 (2017) 208–216.
[18] V. da N. Medeiros, T.C. de Carvalho, E.M. Araújo, H.L. Lira, A.M.D. Leite, E.A. dos Santos Filho, Polyethersulfone nanocomposite membranes with different montmorillonite clays for oil/water separation, Desalin. Water Treat., 154 (2019) 63–71.
[19] K.G. Bhattacharyya, S.S. Gupta. Adsorption of a few heavy metals on natural and modified kaolinite and montmorillonite: a review, Adv. Colloid Interface Sci., 140 (2008) 114–131.
[20] V. Ramamurthi, P.G. Priya, S. Saranya, C.A. Basha, Recovery of nickel (II) ions from electroplating rinse water using hectorite clay, Mod. Appl. Sci., 3 (2009) 37–51.
[21] W.A. Carvalho, C. Vignado, J. Fontana, Ni(II) removal from aqueous effluents by silylated clays, J. Hazard. Mater., 153 (2008) 1240–1247.
[22] M.E. Argun, Use of clinoptilolite for the removal of nickel ions from water: kinetics and thermodynamics, J. Hazard. Mater., 150 (2008) 587–595.
[23] S. Ansanay-Alex, C. Lomenech, C. Hurel, N. Marmier, Adsorption of nickel and arsenic from aqueous solution on natural sepiolite, Int. J. Nanotechnol., 9 (2012) 204–215.
[24] A. Sdiri, T. Higashi, R. Chaabouni, F. Jamoussi, Competitive removal of heavy metals from aqueous solutions by montmorillonitic and calcareous clays, Water Air Soil Pollut., 223 (2012) 1191–1204.
[25] H. Zhang, Z. Tong, T. Wei, Y. Tang, Removal characteristics of Zn(II) from aqueous solution by alkaline Ca-bentonite, Desalination, 276 (2011) 103–108.
[26] P. Vasconcelos, W. Lima, M. Silva, A. Brito, H. Laborde, M. Rodrigues, Adsorption of zinc from aqueous solutions using modified Brazilian gray clay, Am. J. Anal. Chem., 4 (2013) 510–519.
[27] A.L.P. de-Araujo, M.L. Gimenes, M.A.S.D. de-Barro, M.G.C. da-Silva, Kinetic and equilibrium study of zinc removal by brazilian bentonite clay, Mater. Res., 16 (2013) 128–136.
[28] A. Sdiri, M. Khairy, S. Bouaziz, S. El-Safty, A natural clay adsorbent for selective removal of lead from aqueous solutions, Appl. Clay Sci., 126 (2016) 89–97.
[29] A.A. Taha, M.A. Shreadah, A.M. Ahmed, H.F. Heiba, Multi-component adsorption of Pb(II), Cd(II), and Ni(II) onto Egyptian Na-activated bentonite; equilibrium, kinetics, thermodynamics, and application for seawater desalination, J. Environ. Chem. Eng., 4 (2016) 1166–1180.
[30] W.R. Li, X.B. Xie, Q.S. Shi, H.Y. Zeng, Y.S. Ou-Yang, Y.B. Chen, Antibacterial activity and mechanism of silver nano particles on *Escherichia coli*, Appl. Microbiol. Biotechnol., 85 (2010) 1115–1122.
[31] M.B. Đolić, V.N. Rajaković-Ognjanović, S.B. Štrbac, Z.L. Rakočević, Đ.N. Veljović, S.I. Dimitrijević, L.V. Rajaković, The antimicrobial efficiency of silver activated sorbents, Appl. Surf. Sci., 357 (2015) 819–831.
[32] X.F. Zhang, Z.G. Liu, W. Shen, S. Gurunathan, Silver nanoparticles: synthesis, characterization, properties, applications, and therapeutic approaches - review, Int. J. Mol. Sci., 17 (2016) pii: E1534.
[33] K. Taleb, J. Markovski, Z. Veličković, J. Rusmirović, M. Rančić, V. Pavlović, A. Marinković, Arsenic removal by magnetite-loaded amino modified nano/microcellulose adsorbents: effect of functionalization and media size, Arabian J. Chem., 12 (2019) 4675–4693.
[34] D. Budimirović, Z.S. Veličković, V.R. Djokić, M. Milosavljević, J. Markovski, S. Lević, A.D. Marinković, Efficient As(V) removal by A-FeOOH and A-FeOOH/A-MnO2 embedded PEG-6-arm functionalized multiwall carbon nanotubes, Chem. Eng. Res. Des., 119 (2017) 75–86.

[35] Z.S. Veličković, R. Karkalić, Z. Bajić, A. Marinković, A. Nikolić, P. Otrisal, S. Florus, Cerium supported on high porous carbon from fish scales carp, as a novel low cost adsorbent to remove As(V) ions from water, J. Intern. Sci. Pub., 12 (2018) 110–122.
[36] M. Mourabet, A. El Rhilassi, H. El Boujaady, M. Bennani-Ziatni, A. Taitai, Use of response surface methodology for optimization of fluoride adsorption in an aqueous solution by Brushite, Arabian J. Chem., 10 (2017) S3292–S3302.
[37] L. Jiang-Jen, D. Rui-Xuan, T. Wei-Cheng, In: D.P. Perez, High Surface Clay-Supported Silver Nanohybrids, Silver Nanoparticles, InTech Open, 2010, pp. 161–176.
[38] K. Shameli, M.B. Ahmad, M. Zargar, W. Md, Z.W. Yunus, N.A. Ibrahim, Fabrication of silver nanoparticles doped in the zeolite framework and antibacterial activity, Int. J. Nanomed., 6 (2011) 331–341.
[39] N.L. Pacioni, C.D. Borsarelli, V. Rey, A.V. Veglia, Synthetic Routes for the Preparation of Silver Nanoparticles, Silver Nanoparticle Applications, Springer International Publishing Switzerland, 2015, pp. 13–47.
[40] Z.S. Veličković, A. Marinković, Z. Bajić, J. Marković, A. Perić-Grujić, P. Uskoković, M. Ristić, Oxidized and ethylenediamine-functionalized multi-walled carbon nanotubes for the separation of low concentration arsenate from water, Sep. Sci. Technol., 48 (2013) 2047–2058.
[41] Z.S. Veličković, Z. Bajić, M. Ristić, A. Marinković, M. Vuruna, Modification of multi-wall carbon nanotubes for the removal of cadmium, lead and arsenic from wastewater, Dig. J. Nanomater. Bios., 8 (2013) 501–511.
[42] K. Shameli, M.B. Ahmad, A. Zamanian, P. Sangpour, P. Shabanzadeh, Y. Abdollahi, M. Zargar, Green biosynthesis of silver nanoparticles using *Curcuma longatuber* powder, Int. J. Nanomed., 7 (2012) 5603–5610.
[43] S.E. Cabaniss, Forward modeling of metal complexation by NOM: II prediction of binding site properties, Environ. Sci. Technol., 45 (2011) 3202–3209.
[44] K. Ravichandran, N. Nisha Banu, V.S. Selvi, B. Muralidharan, T. Arun, Rectification of sulphur deficiency defect in CdS based films by introducing a novel modification in the SILAR cyclic process, J. Alloys Compd., 687 (2016) 402–412.
[45] A. Shah, Latif-ur-Rahman, R. Qureshi, Zia-ur-Rehman, Synthesis, characterization and applications of bimetallic (Au-Ag, Au-Pt, Au-Ru) alloy nanoparticles, Rev. Adv. Mater. Sci., 30 (2012) 133–149.
[46] G.D. Vuković, A.D. Marinković, M. Čolić, M.Đ. Ristić, R. Aleksić, A.A. Perić-Grujić, P.S. Uskoković, Removal of cadmium from aqueous solutions by oxidized and ethylenediamine-functionalized multiwalled carbon nanotubes, Chem. Eng. J., 157 (2010) 238–248.
[47] M.R. Soares, J.C. Casagrande, E.R. Mouta, Nickel adsorption by variable charge soils: effect of pH and ionic strength, Braz. Arch. Biol. Technol., 54 (2011) 207–220.
[48] H. Qiu, L. Lv, B.C. Pan, Q.J. Zhang, W.M. Zhang, Q.X. Zhang, Critical review in adsorption kinetic models, J. Zhejiang Univ.-Sci. A., 10 (2009) 716–724.
[49] R.M.C. Viegas, M. Campinas, H. Costa, M.J. Rosa, How do the HSDM and Boyd's model compare for estimating intraparticle diffusion coefficients in adsorption processes, Adsorption, 20 (2014) 737–746.
[50] Z.S. Veličković, G.D. Vuković, A.D. Marinković, M.S. Moldovan, A.A. Perić-Grujić, P.S. Uskoković, M.Đ. Ristić, Adsorption of arsenate on iron(III) oxide coated ethylenediamine functionalized multiwall carbon nanotubes, Chem. Eng. J., 181–182 (2012) 174–181.
[51] Q. Wang, D. Zhang, S. Tian, P. Ning, Simultaneous adsorptive removal of methylene blue and copper ions from aqueous solution by ferrocene-modified cation exchange resin, J. Appl. Polym. Sci., 131 (2014), doi: 10.1002/app.41029.
[52] R. Selvakumar, N. Arul Jothi, V. Jayavignesh, K. Karthikaiselvi, G.I. Antony, P.R. Sharmila, S. Kavitha, K. Swaminathan, As(V) removal using carbonized yeast cells containing silver nanoparticles, Water. Res., 45 (2011) 583–592.
[53] K. Taleb, J. Markovski, M. Milosavljević, M. Marinović-Cincović, J. Rusmirović, M. Ristić, A. Marinković, Efficient arsenic removal by cross-linked macroporous polymer impregnated with hydrous iron oxide: material performance, Chem. Eng. J., 279 (2015) 66–78.
[54] J. Febrianto, A.N. Kosasih, J. Sunarso, Y.H. Ju, N. Indraswati, S. Ismadji, Equilibrium and kinetic studies in adsorption of heavy metals using biosorbent: a summary of recent studies, J. Hazard. Mater., 162 (2009) 616–645.
[55] I.A. Shabtai, Y.G. Mishael, Catalytic polymer-clay composite for enhanced removal and degradation of diazinon, J. Hazard. Mater., 335 (2017) 135–142.
[56] B. Xu, G. Gonella, B.G. DeLacy, H.L. Dai, Adsorption of anionic thiols on silver nanoparticles, J. Phys. Chem. C, 119 (2015) 5454–5461.
[57] M.B. Ibrahim, S. Sani, Comparative isotherms studies on adsorptive removal of congo red from wastewater by watermelon rinds and neem-tree leaves, Open J. Phys. Chem., 4 (2014) 139–146.
[58] US Environmental Protection Agency, Ambient Water Quality Criteria for Silver, Washington, D.C., 1980 (EPA 440/5-80-071).
[59] Y.-T. Woo, D. Lai, J.L. McLain, M.K. Manibusan, V. Dellarco, Use of mechanism-based structure-activity relationships analysis in carcinogenic potential ranking for drinking water disinfection by-products, Environ. Health Perspect., 110 (2002) (Suppl. 1, 75–88).
[60] S.P. Deshmukh, S.M. Patil, S.B. Mullani, S.D. Delekar, Silver nanoparticles as an effective disinfectant: a review, Mater. Sci. Eng., C, 97 (2019) 954–965.
[61] C. Marambio-Jones, E.M.V. Hoek, A review of the antibacterial effects of silver nanomaterials and potential implications for human health and the environment, J. Nanopart. Res., 12 (2010) 1531–1551.
[62] E.E. Elemike, D.C. Onwudiwe, A.C. Ekennia, C.U. Sonde, R.C. Ehiri, Green synthesis of Ag/Ag_2O nanoparticles using aqueous leaf extract of *Eupatorium odoratum* and its antimicrobial and mosquito larvicidal activities, Molecules, 22 (2017) 674–689.
[63] C. Carlson, S.M. Hussain, A.M.K. Schrand, L. Braydich-Stolle, K.L. Hess, R.L. Jones, Unique cellular interaction of silver nanoparticles: size-dependent generation of reactive oxygen species, J. Phys. Chem. B, 112 (2008) 13608–13619.
[64] Z.-M. Xiu, Q.-B. Zhang, H.L. Puppala, V.L. Colvin, P.J.J. Alvarez, Negligible particle-specific antibacterial activity of silver nanoparticles, Nano Lett., 12 (2012) 4271–4275.
[65] Guidelines for Drinking-water Quality, 2nd ed., Vol. 2., Health Criteria and Other Supporting Information, World Health Organization, Geneva, 1996. Available at: www.WQA.ORG.
[66] H. Ortiz-Ibarra, N. Casillas, V. Soto, M. Barcena-Soto, R. Torres-Vitela, W. de la Cruz, S. Gomez-Salazar, Surface characterization of electrodeposited silver on activated carbon for bactericidal purposes, J. Colloid Interface Sci., 314 (2007) 562–571.
[67] F.-R.F. Fan, A.J. Bard, Chemical, electrochemical, gravimetric, and microscopic studies on antimicrobial silver films, J. Phys. Chem. B, 106 (2002) 279–287.

Supplementary material

S1. Experimental setup

S1.1. Materials

The montmorillonite clay was collected in its hydrated state directly from deposits located in "Uma" near the village Dojkinci, the municipality of Pirot, Serbia. Bearing in mind that the properties of adsorbents, synthesis reproducibility, adsorption of heavy metal ions, and the reproducibility of experiments depend extensively on the presence of impurities, the following high purity chemicals were used: xylol (mixture o–, m–, and p–isomer of dimethyl benzene), silver nitrate ($AgNO_3$; Sigma Aldrich, p.a.), sodium borohydride ($NaBH_4$; Sigma, p.a.), Cadmium, and Nickel standard solution suitable for atomic absorption spectrometry, 1,000 mg L^{-1} Cd^{2+} (Sigma), Potassium nitrate (KNO_3; Merck, p.a.), Acetone (Sigma Aldrich, p.a.), deionized water (DW; resistivity 18 MΩ cm). Diazinon was kindly provided by Chemical Industry Župa Ltd., Kruševac, Serbia.

S1.2. Adsorbent preparation and optimization procedure

The clay collected from the natural deposits was washed with DW, dried in the air for 24 h, and milled in a ball mill for 6 h to obtain satisfactory grain size of raw montmorillonite clay (raw-Cy) with a developed surface (1–10 μm, 90% according to sieve analysis) useful for subsequent modification. The ground clay was thereafter washed three times with acetone in order to remove organic residues, and dried in an oven for 3 h at 378°K. Obtained material was used for the synthesis of Cy-npAg: Cy-npAg$_{Ch}$ [main text—chemically induced npAg deposition (CID) method] and adsorbent obtained by photochemical reduction of Ag^+ as follow:

General procedure for ultraviolet (UV) irradiation induced npAg deposition on raw-Cy: The npAg/montmorillonite adsorbent was prepared via a simple and environmentally friendly photochemical deposition to obtain Cy-npAg$_{Ph}$ (Ph—designates photochemically induced reduction of silver ion) [S1,S2]. The clay dispersion was prepared by mixing 10 g of montmorillonite in 100 mL of DW at 200 rpm for 10 min. Thus, an aqueous solution of $AgNO_3$ at a concentration of 3.94 mg mL^{-1} was prepared (the equivalent concentration of 2.5 mg mL^{-1} Ag; Table 1). The dispersion of raw-Cy in $AgNO_3$ solution was magnetically stirred at 200 rpm for 120 min, and after irradiated with UV-A light using a Philips 125 W lamp, intensity 12.7 mW cm^{-2}, for 60 min at room temperature. The dispersion was centrifuged at 4,000 rpm for 10 min, and washed with 100 mL of DW (three cycles). Obtained material was filtered and dried in a vacuum at 353°K for 6 h. Other syntheses were analogously performed according to an optimization plan given in Table 1.

To optimize, adsorbent performance response surface methodology (RSM) was applied. Adsorption capacity depends on adsorbents physical and chemical properties predominantly associated with the certain synthesis route. The most influential operational parameter: temperature, time, and volume of $AgNO_3$ solution were chosen/selected in an optimization procedure to obtain the main goal: high adsorption capacity. Optimization of the adsorbent synthesis was carried out by applying an RSM [S3,S4] based on a Box-Behnken rotatable design for three factors. RSM is following one of the main principles of environmental protection where the significant reduction of the experiment number leads to the reduction of the created waste. The coded and operational values of the selected variables are given in Tables S1, together with the experimental plan, comprising 14 experimental runs plus three replicates on the central point [S5].

Each experiment (except the central point) was performed in duplication. The output variable was the adsorption capacity. The data obtained in these experiments were fitted with a second-order polynomial equation and the coefficients of the response function and statistical significance of the process factors and their interactions are assessed by the analysis of variance (ANOVA), using commercial software Design-Expert, Software Version 9 (Stat-Ease, Inc., 2021 E. Hennepin Ave., Suite 480, Minneapolis, USA). The Fisher test was used to determine the adequacy of the model and the Student distribution to evaluate the significance of the coefficients.

Improvement of Cy-npAg$_{Ch}$ synthesis, that is, CID synthesis, was provided by the controllable deposition of npAg in the solvent/nonsolvent (water/xylene) system. A 10 g of the rawCy was soaked with 100 mL of xylene, and placed in a 250 mL round bottom flask provided with the constant flow of nitrogen. Xylene was used as a continual hydrophobic phase to provide selective wetting of clay surface. Optimization of the water quantity necessary for the preparation of $AgNO_3$ solution was performed in a batch system in order to provide covering of clay outer surface. In general, established optimal technology was as follow: a steady mixing 20 mL of $AgNO_3$ solution (39.4 mg mL^{-1} $AgNO_3$; 25.0 mg mL^{-1} Ag) was added in the reactor over a 15 min period via a spray system to provide effective distribution over hydrophilic clay surface (also forced by non-solvent). In that way formation of uniform film at overall clay surface and increase the effectiveness of silver ion transport into pores system. After additional mixing for 15 min, reduction by $NaBH_4$ was performed by spraying 35.72 mL of the $NaBH_4$ aqueous solution (1.75 mg mL^{-1}) was added, and solution was mixed for 60 min. The obtained product was filtered, washed with 200 cm^3 DW, divided in two portions and dried applying either vacuum/drying (VD) or freeze/drying (FD) techniques. The product processed by VD at 40°C for 10 h was named Cy-npAg$_{Ch}$(VD). The steps of FD are as follows, freezing at –30°C for 24 h, followed by drying at –50°C/0.05 mbar for 24 h and at –70°C/0.01 mbar for 1 h. The obtained material was named Cy-npAg$_{Ch}$(FD). Another modification of Cy-npAg$_{Ch}$(FD) synthesis procedure consisted of stepwise addition of $AgNO_3$ solution (3°× 4 mL) followed by FD to intermediary and final products, and thus obtained adsorbent was named Cy-npAg$_{Ch}$(FD-5).

S1.3. Characterization and pollutant determination methods

The synthesized adsorbent was characterized by using different instruments. The specific surface area, specific pore volume, and pore diameter were determined by the Brunauer-Emmett-Teller (BET) method of nitrogen adsorption/desorption at 77.4°K, using the gas adsorption analyzer Micromeritics ASAP 2020MP V 1.05 H (Micromeritics Instrument Corporation 4356 Communications Drive, Norcross, GA 30093 USA).

Table S1
Box-Behnken experimental plan for RSM in coded and real factor values for the diazinon removal by Cy-npAg$_{Ch}$ ($C_{i[diazinon]}$ = 30 mg L^{-1}; m/V = 125 mg L^{-1}; pH = 6.5)

Exp. no.	T (A)	t (B)	V_{AgNO3} (C)	$q_{(diazinon)}$ mg g^{-1} (response)
1	+1	0	0	77.97611
2	–1	+1	+1	63.79864
3	–1	0	0	63.79864
4	0	–1	0	42.1689
5	+1	–1	–1	36.49791
6	–1	–1	+1	42.1689
7	+1	+1	–1	43.58665
8	0	0	–1	58.12765
9	0	0	+1	77.97611
10	–1	–1	–1	29.40917
11.	0	+1	0	56.7099
12	0	0	0	70.88738
13	+1	–1	+1	70.88738
14	0	0	0	70.88738
15	–1	+1	–1	43.95017
16	+1	+1	+1	77.97611
17	0	0	0	70.88738

Encoded	Actual values of the model		
–1	298°K	30 min	40 mL
0	323°K	60 min	120 mL
+1	348°K	90 min	200 mL

Chemical analysis of adsorbent was performed using Thermo Scientific™ Niton™ XL3t XRF 950 GOLDD+ Analyzer (Thermo Scientific, Thermo Fisher Scientific, Waltham, Massachusetts, USA).

The infrared spectra were recorded with a FTIR (Fourier transform infrared spectroscopy) in transmission mode between 400 and 4,000 cm^{-1}, at a resolution of 4 cm^{-1} using a BOMEM spectrometer (Hartmann and Brown) (Bomem Inc./ Hartmann & Braun. 450 Saint-Jean-Baptiste Ave. Quebec, Canada). The FTIR spectra were recorded before and after the adsorption at room temperature.

The phase and structural analysis were characterized using X-ray diffraction (XRD; BRUKER D8 ADVANCE), with Vario 1 focusing primary monochromator, Cu Kα source in the range 10°C–90°C, step size of 0.01°C at room temperature (BRUKER, Billerica, Massachusetts, USA).

To analyze morphology of synthesized adsorbents the scanning electron microscopy (SEM) SUPRA 35 VP (Carl Zeiss, Germany) was used.

A laboratory pH meter, Mettler Toledo FE20/FG2 (Switzerland), with the accuracy of ±0.01 pH units, was used for pH measurements. The pH values at the point of zero charge, that is, the pH above which the total surface of the samples is negatively charged, were measured using the pH drift method, before and after adsorption [S6].

The concentration of heavy metal ions in the solution was analyzed by the inductively coupled plasma mass spectrometry (ICP-MS) according to the literature method using an Agilent 7500ce ICP-MS system (Waldbronn, Germany) equipped with an octopole collision/reaction cell, Agilent 7500 ICP-MS ChemStation software, a MicroMist nebulizer and a Peltier cooled (2°C) quartz Scott type double pass spray chamber. Standard optimization procedures and criteria specified in the manufacturer's manual were followed

S1.4. Adsorption and kinetic experimental conditions, and error functions

The adsorption of heavy metal ions, Cd^{2+} and Ni^{2+} were studied in a batch system as it was described in recent studies [S7–S9]. A mass of the material to be tested: 1.0, 2.0, 3.0, 4.0, 6.0, 8.0, and 10.0 mg (ratio of adsorbent/volume of solution was m/V = 0.2–2 g/dm^3) was added to glass vial of 10 mL, then 5 mL of a heavy metal solution of 5 mg L^{-1}, obtained by dilution of standard solution, was added or a diazinon solution of a concentration of 30 mg L^{-1}. The following parameters were varied in the adsorption experiment: adsorbent mass, contact time, temperature, and pH value. To improve the contact between the solid phase (adsorbent) and the liquid phase, the dispersion was ultrasonically treated. The eluent was separated from the adsorbent by filtration in a vacuum through a PTFE filter with a 0.22 μm pore diameter. The concentration of the diazinon was followed at 245 nm using UV-VIS spectrophotometry (Shimadzu 1800, Japan) and high-performance liquid chromatography (SpectraSystem UV1000). The heavy metal ions were analyzed using ICP-MS. Comparative adsorption experiments were performed in dark at the following condition: m/V = 0.2 g/dm^3, concentration of diazinon solution 30 mg L^{-1} and T = 298°K.

The capacity of the adsorbent is calculated according to the following Eq. (S1):

$$q = \frac{C_i - C_e}{m} V \tag{S1}$$

Whereas q is adsorbent capacity in mg g^{-1}, C_i and C_f are the initial and final (equilibrium) concentrations of heavy metal ions in mg L^{-1}, V is volume solution in L, and m is adsorbent mass in g. The effect of the temperature (298°K, 308°K, and 318°K) on the adsorption of heavy metals (Cd^{2+} and Ni^{2+}) was tested at pH 6 and 8 at optimum contact time of the adsorbent with the desired mass.

The influence of the contact time on the adsorption of heavy metals was also tested, since the initial concentration, the pH, and the temperature were kept constant at varied rates of time duration of the adsorption process (sample was taken at t_0 = 5 min, interval 5 min, and t = 90 min). Testing the influence of the pH value to the process of the adsorption experiments were performed in a range on the preferred mass of the adsorbent at a starting concentration of $C_{i\left[Cd^{2+}\text{and } Ni^{2+}\right]}$ = 5.0 mg dm^{-3}, $C_{i[diazinon]}$ = 30.0 mg dm^{-3}, and m/V = 2 g dm^{-3}. Comparative kinetic experiments were performed in dark at the following condition: m/V = 2 g/dm^3, concentration of diazinon solution 30 mg L^{-1} and T = 298°K.

Errors and the values of the correlation coefficient (R^2) calculated from the regression analysis were determined to find which isothermal and kinetic model is best to describe the results obtained by the adsorption. A regression analysis was performed by linear and non-linear regression, to best

fit the experimental results with the theoretical assumption of an isothermal model. The results were analyzed using normalized standard deviation $\Delta q/\%$, which were calculated according to the following Eq. (S2):

$$\Delta q(\%) = \sqrt{\sum \frac{\left[\left(q_{exp} - q_{cal}\right)/q_{exp}\right]^2}{N-1}} \times 100 \quad \text{(S2)}$$

Whereas q_{exp} and q_{cal} are experimental and calculated amounts of adsorbed heavy metal ions on the adsorbent; N is the number of data used in the analysis.

All experiments were performed in triplicate and given as average values. The maximum deviation is <3% (experimental error). All calculated errors for isotherm, kinetic, and thermodynamic parameters were determined using commercial software (Microcal Origin 8.0) in a nonlinear regression program.

Leachability testing was performed according to standard Toxicity Characteristic Leaching Procedure [S10].

S1.5. Antimicrobial activity

The antibacterial activity of the Cy-npAg$_{Ch}$, in vitro study, was estimated from the results of the disk diffusion method, using Mueller–Hinton agar (MHA). The bacterial suspension was adjusted to match the tube of the 0.5 McFarland turbidity standards using the 600 nm spectrophotometer (equals 1.5 × 10^8 colony-forming units/mL). The surface of MHA was completely inoculated, and the impregnated disks were placed on the inoculated agar and incubated at 37°C for 24 h. After incubation, the diameter of the growth of the inhibition zones was measured. Determination of inhibition zones in millimetres (mm) was performed according to the recommended standards of the National Committee for Clinical Laboratory Standards (now renamed Clinical and Laboratory Standards Institute, 2000). *Staphylococcus aureus* ATCC29213, *Escherichia coli* ATCC 25922, and *Pseudomonas aeruginosa* ATCC 15442 were used for the antibacterial effect assay. Chloramphenicol was used as the positive standards in order to control the sensitivity of the bacteria. All tests were done in triplicate [S2].

S1.6. Modeling of ionic speciation

MINTEQ is a computer program, used for surface complexation computation combining the best features of two models: mathematical structure from MINEQL [S11] and thermodynamic data base, temperature correction of equilibrium constants using either the Van't Hoff relationship and ionic strength correction using either the extended Debye-Hückel equation or the Davies equation from WATEQ3 [S12].

S1.7. Modeling of diazinon structure

Preliminary semi-empirical screening for the most labile chemical bond of methomyl was done using PM6 method [S13]. The lowest energy diazinon structure was used for further molecular electrostatic potential (MEP) visualization. VEGA ZZ 3.1.2 was used as a graphical user interface [S14].

S2. Results and discussion

S2.1. Optimization of adsorbent synthesis

Temperature of the reaction mixture during the adsorbent synthesis ($X1$), the reaction time ($X2$), and the volume of $AgNO_3$ solution ($X3$) were optimized to obtain the maximum adsorption capacity toward diazinon. The Cy-npAg$_{Ch}$ adsorbent was obtained by reductive precipitation of silver oxide nanoparticle on raw-Cy surface using $NaBH_4$. At first, the results of the analysis were optimized by the software Design-Expert 9 showing that the optimal experimental condition for silver oxide nanoparticles deposition was obtained using 10 g of raw-Cy and 40, 120, or 200 mL of $AgNO_3$ aqueous solution at a concentration of 3.94 mg mL^{-1} (the concentration equivalent of 2.5 mg mL^{-1} Ag) and 90 mL of the $NaBH_4$ at 323°K for 45 min. The maximum of adsorption capacities was obtained at 4.4% silver nanodeposite loading on raw-Cy. Higher silver loading contributes to increase of unfavorable weight/surface active sites ratio and noticeable decrease of adsorption capacity at Ag > 5% loading.

RSM was used to examine the effects of the variables and to find the optimal combination of variables on the amount of adsorbed metal that will give the highest amount of adsorbed diazinon. The interactions between process variables and responses were determined by ANOVA. Polynomial model terms were evaluated at the 99% confidence level by P-value (probability). P-values and q_m (mg g^{-1}) value were given in Table S2 according to adsorbent Cy-npAg$_{Ch}$ for diazinon. P-value is the smallest significance level that allows rejection of the null hypothesis. Generally, the smaller the P-value related to the coefficient of the term the more important it is. When the P-value is <0.05, model and model terms are statistically significant with 95% reliability, and when the P-value <0.01 model and model term is significant with 99% reliability [S1]

Detailed explanation on the use of the presented methodology is given in Supplementary material. Variation analysis examined the importance of different variables (adsorbent mass, m; adsorption time, t; temperature, T) on the adsorption. Estimated model equations for Cy-npAg$_{Ch}$

Table S2
ANOVA for the surface quadratic model of the response to the removal of diazinon from water using the Cy-npAg$_{Ch}$

Terms	P-value	Mean square	F-Value	p-value prob > F
Model	<0.0001	435.98	98.44	<0.0001
$A(T)$	<0.0001	407.03	91.91	<0.0002
$B(t)$	<0.0001	421.06	95.08	<0.0001
$C(V)$	<0.0001	1,469.81	331.88	<0.0001
Value model				
R-Squared	0.9933			
Adj. R-Squared	0.9832			
Pred. R-Squared	0.9252			
Adeq. precision	31.399			

adsorbent are graphically depicted in the form of 3-D surface plots and contour plates for diazinon (Fig. S1).

The removal of diazinon is presented in Table 1. The model *F*-value of 98.44 implies the model is significant. There is only a 0.01% chance that a "Model *F*-Value" this large could occur due to noise. Values of "prob > *F*" <0.0500 indicate model terms are significant. In this case *A*, *B*, and *C* are significant model terms. Values >0.1000 indicate the model terms are not significant. If there are many insignificant model terms (not counting those required to support hierarchy), model reduction may improve the model. The "Predicted *R*-Squared" of 0.9252 is in reasonable agreement with the "Adjusted *R*-Squared" of 0.9832. "Adequate Precision" measures the signal to noise ratio. A ratio >4 is desirable. The model ratio of 31.399 indicates an adequate signal. This model can be used to navigate the design space.

S2.2. Physical and chemical characterization of the adsorbent

Applied methodologies [BET, X-ray fluorescence (XRF), FTIR, XRD, and SEM analysis] provided means for controlled precipitation of silver nanoparticle (npAg) deposit with improved textural properties, that is, beneficial morphology/chemistry with a number of available adsorptive useful for heavy metal ions removal. Chemical analysis of the adsorbent was performed using the XRF analyzer, the results of the analysis are given in Table S2.

The chemical composition of the clay is typical for the wider region (Serbia, Bosnia and Herzegovina, Turkey) which contains a higher content of SiO_2, which may contribute to the improvement of adsorption characteristics as it was indicated in the studies [S20,S22–S24].

S2.3. Characterization of adsorbent functionalities – FTIR analysis

FTIR is a useful tool in identifying the presence of functional groups in the molecule as well as in chemical bonds, often demonstrating unique adsorption energy for each functional group or bond. FTIR spectra of raw clay and clay doped with npAgs Cy-npAg$_{Ch}$ before and after the adsorption of Cd^{2+} and Ni^{2+} ions are shown on Fig. S2. Due to the fact that only small changes in peak intensity and shifts were observed in the FTIR spectra after the adsorption of Cd^{2+} and Ni^{2+} ions, they are not presented here.

The FTIR spectra of raw-Cy and Cy-npAg$_{Ch}$ are shown in Fig. S1. The FTIR pattern of raw-Cy, display sharp peaks at 1,045; 917; 845; and 531 cm^{-1} which are characteristic peaks of montmorillonite [S21]. The overlapped absorption peak in the region of 1,654 cm^{-1} is assigned to the –OH bending mode of the adsorbed water and hydroxyl present of the clay surface. The absorption bands in the region 700–1,400 cm^{-1} are primarily assigned to the stretching vibration of the Si–O–Si bonds and the deformation modes of OH groups present at the crystallite surface of different oxides (Al^{3+}, Fe^{3+}, and Mg^{2+}). The band observed at 917 cm^{-1} is assigned to OH groups attached to Al^{3+} ions. The characteristic peak at 1,138 cm^{-1} is due to the Si–O–Si stretching and out of plane Si–O–Si deformation mode of the montmorillonite. The band at 1,045 cm^{-1} is assigned to the Si–O–Si stretching (in plane) vibration for layered silicates. The band in the region of 873 cm^{-1} is due to the Si–O–Al stretching mode of the montmorillonite. The peaks at 531 cm^{-1} are assigned to the Si–O–Al bending vibration [S22–S25]. The new FTIR peaks at Cy-npAg$_{Ch}$ at 984 and 615 cm^{-1} are assigned stretching vibration Ag-C [S18]. The FTIR spectra indicate the inflexibility of the silicate layers and the non-bond chemical interface between the silicate layers as well as the npAgs (npAg) in Cy-npAg$_{Ch}$. These results confirm that due to the existence of van der Waals interactions between the oxygen groups of montmorillonite and npAg cause shifting to low wave numbers and the intensity change of the peak at 1,457 cm^{-1} [S8]. The interactions between the hydroxyl groups of montmorillonite

Table S3
Chemical composition[a] of raw-Cy of different origin, and Cy-npAg$_{Ch}$ adsorbents

Place and state of origin/oxide	Dojkinci, Serbia		Czech Republic	China	Tokat Re şadiye deposit of Turkey	Crni Timok; Serbia	Cheto, Arizona, USA	Gerzovo, BiH	province of Río Negro (Argentina)
	Raw-Cy	Cy-npAg$_{Ch}$	[S15]	[S16]	[S17]	[S18]	[S19]	[S20]	[S21]
SiO_2	70.32	69.72	57.00	61.02	57.09	59.42	69.08	52.88	53.40
Al_2O_3	16.76	16.77	17.30	18.54	16.73	16.01	19.71	23.72	17.95
Fe_2O_3	2.44	2.31	1.00	1.69	3.24	1.99	1.75	6.80	4.75
CaO	2.97	2.24	–	2.60	3.18	1.20	2.09	1.83	1.08
MgO	4.05	3.82	–	5.7	–	2.49	6.91	–	2.80
Na_2O	0.79	0.35	0.40	3.00	2.51	0,28	0.07	0.02	3.35
K_2O	0.58	0.14	1.20	0.77	–	0,60	–	–	0.26
TiO_2	0.15	0.13	6.30	0.11	–	0.14	0.26	0.83	0.37
P_2O_5	0.04	0.01	0.10	–	–	–	–	–	0.05
MnO	0.09	0.03	0.30	–	–	0.01	0.05	–	0.01
LiO_2	–	–	0.10	–	–	–	–	–	–
Ag	–	3.66	–	–	–	–	–	–	–

[a]all elemental content are presented as oxides in mass percent (wt.%)

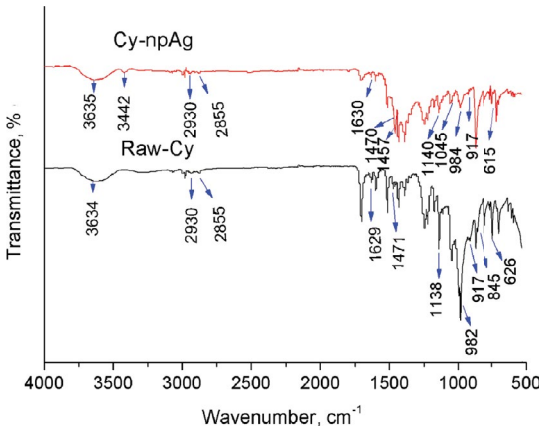

Fig. S1. FTIR spectra of raw clay and clay doped with npAgs Cy-npAg$_{Ch}$.

and npAg was associated with the peak at 3,442 cm^{-1}, and the partial positive charge on the surface of npAg [S26,S27].

S2.4. XRD analysis

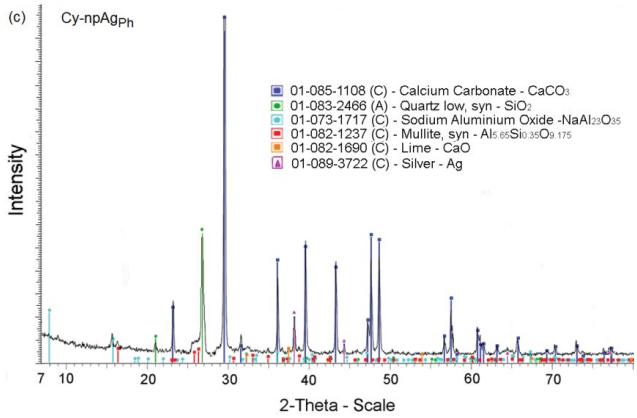

Fig. S2. XRD patterns of the Cy-npAg$_{Ph}$ adsorbent.

S2.5. Effect of pH on the adsorption of the diazinon and Cd^{2+} and Ni^{2+} ions

Speciation diagram of Cd^{2+} and Ni^{2+} are given on Fig. S3.

Cadmium speciation in water could be present by equilibria of different forms of Cd^{2+}, $Cd(OH)^{+}$, $Cd(OH)_2$, $Cd(OH)_3^{-}$, and $Cd(OH)_4^{2-}$ vs. solution pH. Equilibrium concentrations of Cd^{2+} ionic species and precipitation products, that is, cadmium containing species could be calculated from equilibrium constants (log*K*) for hydrolysis reactions at 25°C and the precipitation constant of $Cd(OH)_2(s)$ (1.69×10^{-14}; given on Fig. S3). Removal efficiency of Cd^{2+} at pH higher than 8 as a result of both Cd^{2+} adsorption and co-precipitation of $Cd(OH)^{+}$, $Cd(OH)_2$ up to pH 11, and after only precipitation of $Cd(OH)_2$ at pH > 11 dominate.

In contrast to the chemical properties of cation, diazinon is an organophosphate insecticide with the structure:

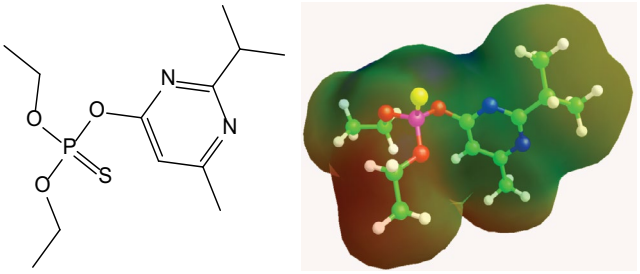

Fig. S4. Diazinon structure and MEP surface.

which possess the miscellaneous electrostatic potential to establish physical/chemical bonds with Cy-npAg$_{Ch}$ surface functionalities/charges.

MEP analysis was used to evaluate and visualize charge distribution over investigated compounds and illustrate the three-dimensional charge distributions overall investigated molecules. The evaluation of the electrostatic potential at the surface is represented by different colors; blue represents regions of most electronegative electrostatic potential, it indicates the region of high electron density; brown represents regions of the most positive electrostatic potential, that is, region of low electron density. The blue color indicates the

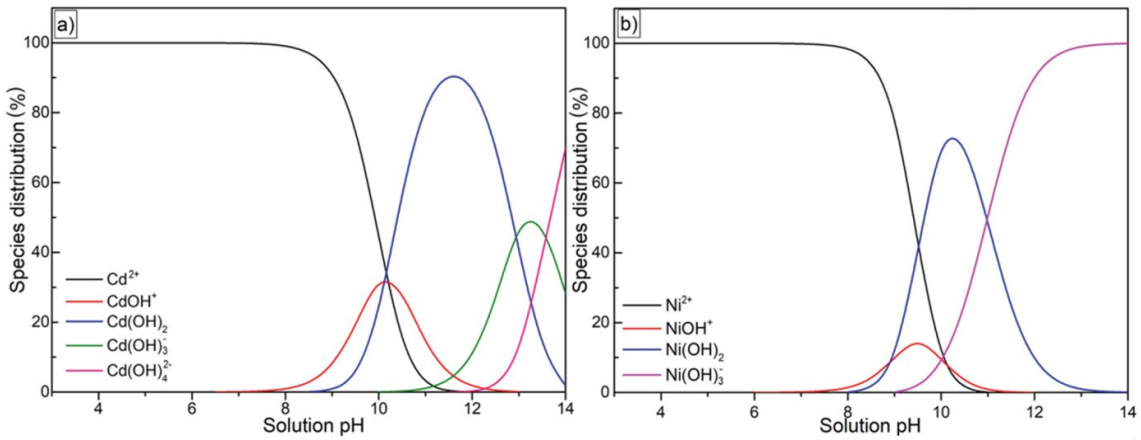

Fig. S3. Speciation of (a) Cd^{2+} and (b) Ni^{2+} obtained using MINTEQ. 3.0 software (C = 25 mg L^{-1}, T = 308°K).

region with strong attractive potential, region favorable for interactions with the positive adsorbent surface.

Similar behavior of Ni^{2+} ionic vs. pH could be observed from Fig. S5 and a significant drop of adsorption efficiency is due to repulsion between the negative adsorbent surface and $Ni(OH)_3^-$ at pH > 10.

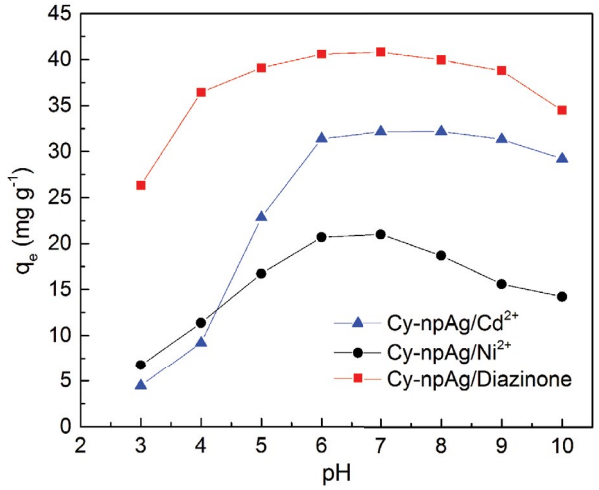

Fig. S5. Influence of pH on adsorption of Cd^{2+} and Ni^{2+} ion and diazinon onto Cy-npAg$_{Ch}$ ($C_{i[Cd^{2+}\text{and } Ni^{2+}]}$ = 5.00 mg L^{-1}, $C_{i[Diazinon]}$ = 30.00 mg L^{-1}; m/V = 200 mg L^{-1}, T = 298°K)

S2.6. Effect of the contact time on the adsorption of diazinon, Cd^{2+}, and Ni^{2+} ions

The effect of time on the adsorption of Diazinon and $Ni^{2+}$and Cd^{2+} ions was analyzed in the range from 5 to 720 min, and 120 min was found to be an appropriate period in a kinetic study (Fig. S6). Among two methods used in adsorption experiments, the system stimulated by sonication showed higher efficiency than conventional mixing. The presence of an ultrasonic field increases the speed of the adsorption due to the reduced resistance to mass transfer. Ultrasonic waves and the bubbles caused by the side effects of cavitation in a solid (adsorbent) generate micro disturbances, thus reducing the boundary layer and increasing the efficiency of mass transfer. In fact, these increase the affinity of the adsorbate to the adsorbent. In this case here, ultrasound does not alter the process of adsorption nor shift the equilibrium to lower concentrations [S28,S29].

S2.7. Effect of the contact time on the adsorption of diazinon, Cd^{2+}, and Ni^{2+} ions

S2.7.1. Adsorption kinetics

The study of kinetics provides an insight into the possible mechanism of adsorption along with the reaction pathways. The adsorption data were analyzed by linear, non-linear least-squares and graphic method in the form of pseudo-first, pseudo-second-order (PSO; Lagergren) and second-order model (Table S4). Diffusion models as Weber–Morris, were

Table S4
Kinetic model equations

Kinetic model	Nonlinear form	Linear form	Equation
Pseudo-first-order equation (Lagergren)	$q = q_e\left(1-e^{-k_1 t}\right)$	$\ln\left(q_e - q\right) = \ln q_e - k_1 t$	(S3)
Pseudo-second-order equation (Lagergren)	$q = \dfrac{t}{\dfrac{1}{k_2 q_e^2} + \dfrac{t}{q_e}}$	$\dfrac{t}{q} = \dfrac{1}{k_2 q_e^2} + \dfrac{1}{q_e} t$	(S4)
Second-order	$q = \dfrac{t}{\dfrac{1}{k_2 q_e^2} + \dfrac{t}{q_e}}$	$\dfrac{t}{C_t} = k_2 t^{\circledcirc} + \dfrac{1}{C_0}$	(S5)
Weber–Morris model (W–M)	$q = k\sqrt{t} + C$		(S6)
Dunwald–Wagner model	$\dfrac{q}{q_e} = 1 - \dfrac{6}{\pi^2}\sum_{n=1}^{\infty}\dfrac{1}{n^2}\exp\left[-n^2 K\, t\right]$ $\log\left(1-\left(\dfrac{q}{q_e}\right)^2\right) = -\dfrac{K}{2.303} t$		(S7)
Homogenous solid diffusion model	$\dfrac{\partial q}{\partial t} = \dfrac{D_s}{r^2}\dfrac{\partial}{\partial r}\left(r^2\dfrac{\partial q}{\partial r}\right)$ $\dfrac{q}{q_s} = 1 + \dfrac{2R}{\pi r}\sum_{n=1}^{\infty}\dfrac{(-1)^n}{n}\sin\dfrac{n\pi r^{\circledcirc}}{R}\exp\left[\dfrac{-D_s\, t\,\pi^2 n^2}{R^2}\right]$		(S8)

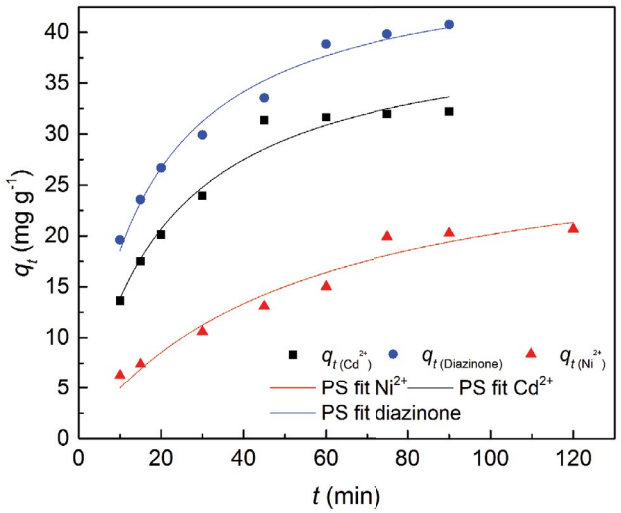

Fig. S6. Time dependent adsorption of diazinon and Cd^{2+} and Ni^{2+} onto Cy-npAg$_{Ch}$ ($C_{i[Cd\ and\ NI]}$ = 5.00 mg L^{-1}; $C_{i[Diazinon]}$ = 30.00 mg L^{-1}; m/V = 200 mg L^{-1}, T = 298°K, pH = 6.5)

used for modeling diffusional processes/limiting step of overall process (Table S4) [S3,S9,S30,S31].

S2.7.2. Activation energy of the adsorption

Activation energy for arsenate adsorption was calculated using Arrhenius Eq. (S9):

$$k_2 = k_0 \exp\left[\frac{-E_a}{RT}\right] \tag{S9}$$

Where k_2 (g mg^{-1} min^{-1}) is the PSO rate adsorption constant, k_0 (g mmol^{-1} min^{-1}) is the temperature independent factor, E_a (kJ mol^{-1}) is the activation energy, R (8.314 J mol^{-1} K^{-1}) is the gas constant and T (K) is the adsorption absolute temperature. A plot of lnk' vs. 1/T gave a straight line with slope $-E_a/R$ from which activation energy was calculated.

The linear form of the Arrhenius equation is given by Eq. (S10):

$$\ln k' = -\frac{E_a}{RT} + \ln A \tag{S10}$$

where k' is the reaction speed constant at the selected temperature, E_a denotes activation energy, R is a universal gas constant (8.314), T is the temperature in Kelvin, and A is the Arrhenius factor (frequency for the given reaction).

S2.8. Adsorption study

The state of interaction/bonding on the solutes/adsorbent surface can be recorded by fitting experimental data with various adsorption isotherms [S30]. The equilibrium adsorption data were fitted by the isotherm models Langmuir, Freundlich, Temkin, and Dubinin–Radushkevich isothermal models [S3,S6,S32]. The Langmuir equation is based on assumption that a point of maximum adsorption corresponds to a saturated monolayer of adsorbate molecules on the adsorbent surface—where the energy of adsorption remains constant and no transfer of the adsorbate in the plane of the surface occurs. The Freundlich sorption isotherm, widely and reliably utilized as a mathematical determining expression, allows for a calculation encompassing surface heterogeneity and an exponential distribution of active sites as well as their respective energies [S6,S30]. Temkin conceived this equation for subcritical vapors in micropore solids where the adsorption process follows a pore filling mechanism onto the energetically non-uniform surface. Temkin isotherm is based on the assumption that the decline of the heat of sorption as a function of temperature is linear rather than logarithmic. The Dubinin–Radushkevich model for subcritical vapors in micropore solids where the adsorption process follows a pore filling mechanism onto the energetically non-uniform surface [S6,S30]. Equations of adsorption isotherms models presented in Table S6.

In adsorption isotherms (Table S6) C is equilibrium metal ion concentration left in the solution (mol L^{-1}); q is adsorbed amount of metal ions (mol g^{-1}); q_{max} and b are Langmuir constants related on the adsorption capacity and adsorption energy. Maximum adsorption capacity, q_{max}, denotes the amount of adsorbate, so the complete adsorption surface is covered with adsorbate monolayer (mol g^{-1}), and b (L mol^{-1}) is the constant related with the adsorption heat. The calculation

Table S5
Second-order model parameters for the adsorption of Cd^{2+}, Ni^{2+}, and diazinon on Cy-npAg$_{Ch}$ ($C_{i[Cd\ and\ Ni]}$ = 5.00 mg L^{-1}; $C_{i[Diazinon]}$ = 30.0 mg L^{-1}; pH = 6.5; m/V = 200 mg L^{-1}).

	Adsorbate	q_e/mg g^{-1}	k_2/g (mg min)$^{-1}$	Δq/%	R^2
Cd^{2+}	298°K	39.930	0.070356	1.78	0.967
	308°K	39.991	0.07606	1.96	0.966
	318°K	40.091	0.082771	2.19	0.965
Ni^{2+}	298°K	30.013	0.066105	4.11	0.864
	308°K	26.705	0.07223	4.02	0.870
	318°K	24.890	0.07967	3.95	0.877
Diazinon	298°K	48.321	0.002255	3.42	0.934
	308°K	48.502	0.002681	2.91	0.954
	318°K	48.823	0.003266	3.78	0.908

Table S6
Adsorption isotherms equations

Isotherms	Nonlinear form	Linear form	Equations
Langmuir	$q = \frac{q_m K_L C}{1 + K_L C}$	$\frac{C}{q} = \frac{1}{K_L q_m} + \frac{C}{q_m}$	(S11)
Freundlich	$q = K_F C^{1/n}$	$\log q = \log K_F + \frac{1}{n}\log C$	(S12)
Temkin	$q_e = \frac{RT}{b}\ln\left(AC_e\right)$	$q_e = \frac{RT}{b}\ln A + \frac{RT}{b}\ln C_e$	(S13)
Dubinin–Radushkevich	$q_e = q_m \exp\left(-B\left(RT\right)^2\left(\ln\left(1+\frac{1}{C_e}\right)\right)^2\right)$	$\ln q_e = \ln q_m - B\left(RT\right)^2\left(\ln\left(1+\frac{1}{C_e}\right)\right)^2$	(S14)

of separation factor according to Eq. S15 based on Langmuir isotherm parameter K_L, indicates adsorption feasibility on the given adsorbent.

$$R_L = \frac{1}{\left(1 + K_L C_0\right)} \quad \text{(S15)}$$

Where C_0/mol L^{-1} is the initial adsorbate concentration and K_L/L mol^{-1} is the Langmuir constant. In Freundlich model, (Eq. S12) K_f (mol^{1-n} L^n/g) is an approximate indicator of the adsorption capacity for the equilibrium concentration, and $1/n$ is the Freundlich adsorption intensity parameter, that is, it defines the strength of adsorption. For $n = 1$ the partition between the two phases are independent of the concentration, $1/n < 1$ indicates normal adsorption, while for $1/n > 1$

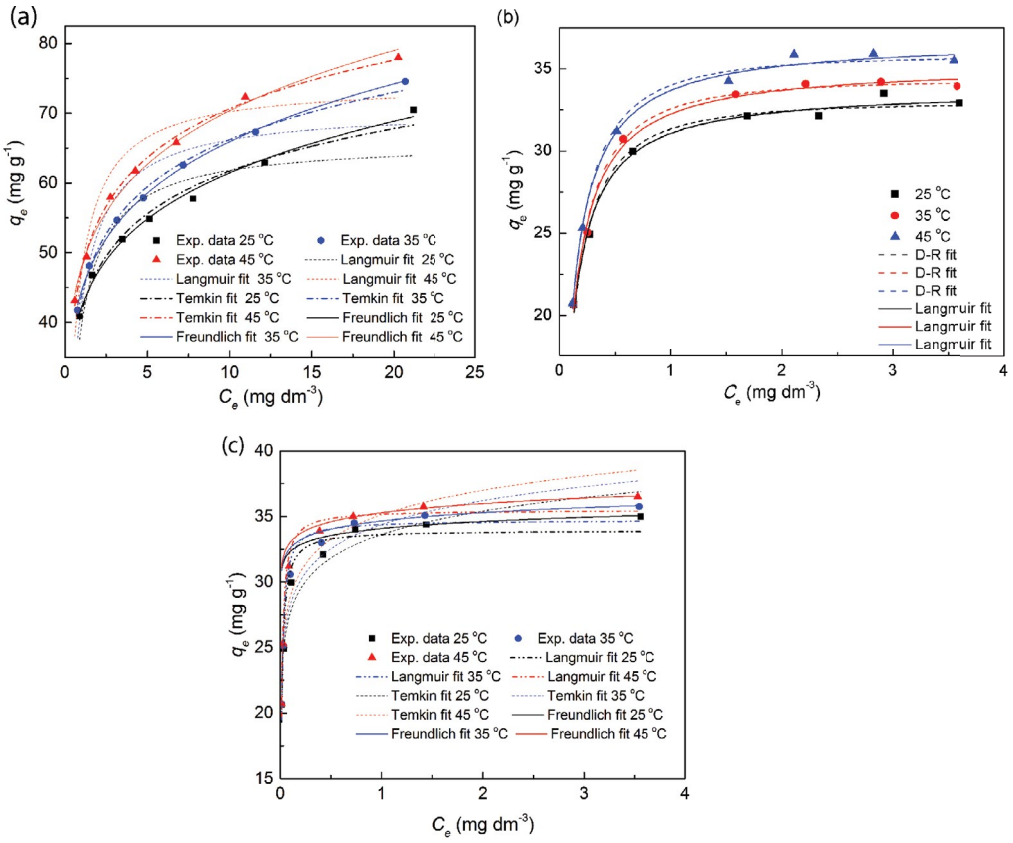

Fig. S7. Fitting of adsorption experimental data with used isotherm models. (a) adsorption of diazinon on Cy-npAg$_{Ch}$ $C_{i[\text{Diazinon}]}$ = 30.00 mg L^{-1}, pH = 6.5, (b) adsorption of Cd^{2+} ions on Cy-npAg$_{Ch}$, $C_{i[\text{Cd}]}$ = 5.00 mg L^{-1}, pH = 6.5, and (c) adsorption of Ni^{2+} ions on Cy-npAg$_{Ch}$, $C_{i[\text{Ni}]}$ = 5.00 mg L^{-1}, pH = 6.5.

Table S7
Efficiency of pollutant removal by Cy-npAg$_{Ch}$ from real water sample (pH ~ 6.6)

Wastewater before treatment		Wastewater after treatment	
ions	mg L^{-1}	mg L^{-1}	Removal %
Pb^{2+}	8.2	3.7	55
Fe^{3+}	15.3	8.2	46
Al^{3+}	0.2	0	100
Ca^{2+}	52	42.2	19
Mg^{2+}	22	8.9	60
Cd^{2+}	0.04	0	100
Ni^{2+}	0.12	0.03	75
Zn^{2+}	55	11	80
Cr(VI)	0.09	0	100
As(V)	1.2	0.32	73
SO_4^{2-}	46	38.2	17
Cl^-	21	20	5

indicates cooperative adsorption. The adsorption parameters calculated using Eq. (S12), the adsorption capacity, q_{max}, and affinity, b, are the most important ones used for the analysis of adsorption process and selection of operational conditions. Design of efficient adsorption technology to achieve moderate water purity will be design to operate to near the saturation point. It implicates adsorption capacity as a major decisive parameter. In the other case, if the requirement is aimed at obtaining high water purity, the adsorption technology should be design to operate "at the left side of the adsorption isotherm," and the adsorption affinity is a decisive factor for technology definition.

S2.8.1. Adsorption thermodynamic

Gibbs free energy ($\Delta G°$), enthalpy ($\Delta H°$), and entropy ($\Delta S°$) were calculated using Van't Hoff thermodynamic Eqs. (S16) and (S17) [S30]

$$\Delta G° = -RT\ln\left(K_L\right) \tag{S16}$$

$$\ln\left(K_L\right) = \frac{\Delta S^0}{R} - \frac{\Delta H^0}{\left(RT\right)} \tag{S17}$$

Where T is the absolute temperature in K, and R is the universal gas constant (8.314/J mol^{-1} K^{-1}) and the adsorption constant K_L was calculated using Langmuir isotherm (Table VI). $\Delta H°$ and $\Delta S°$ were calculated from slopes and interceptions in diagram $\ln(K_L)$–T^{-1}, assuming adsorption kinetics to be stationary.

S2.8.2. Effect of interfering ions

Natural water from the area of the city of Zrenjanin (summer 2018, located in Vojvodina, Serbia) was used for evaluation of Cy-npAg$_{Ch}$ capability for cations/anions removal at the competitive condition. Before the adsorption oxidation process by air, bubbling was performed to provide As(III) and Cr(III) oxidation. Effect of interfering anions showed a significant influence on the decrease of the efficiency of all studied ions removal (Table S7). Tolerable limit was defined as the highest amount of foreign ions that produced an error not exceeding ±5% in the determination of analyte ions.

References

[S1] M. Mourabet, A. El Rhilassi, H. El Boujaady, M. Bennani-Ziatni, A. Taitai, Use of response surface methodology for optimization of fluoride adsorption in an aqueous solution by Brushite, Arabian J. Chem., 10 (2017) S3292–S3302.

[S2] K. Shameli, M.B. Ahmad, M. Zargar, W.Md.Z.W. Yunus, N.A. Ibrahim, Fabrication of silver nanoparticles doped in the zeolite framework and antibacterial activity, Int. J. Nanomed., 6 (2011) 331–341.

[S3] M. Karanac, M. Đolić, Đ. Veljović, V. Rajaković-Ognjanović, Z. Veličković, V. Pavićević, A. Marinković, The removal of Zn^{2+}, Pb^{2+}, and As(V) ions by lime activated fly ash and valorization of the exhausted adsorbent, Waste Manage., 78 (2018) 366–378.

[S4] S. He, F. Zhu, L. Li, W. Ren, Box–Behnken design for the optimization of the removal of Cr(VI) in soil leachate using nZVI/Ni bimetallic particles, Soil Sediment Contam. Int. J., 27 (2018) 658–673.

[S5] M. Castro, A. Martinez, A. Gil-Villegas, Modelling adsorption isotherms of binary mixtures of carbon dioxide, methane and nitrogen, Adsorpt. Sci. Technol., 29 (2011) 59–70.

[S6] D. Budimirović, Z.S. Veličković, V.R. Djokić, M. Milosavljević, J. Markovski, S. Lević, A.D. Marinković, Efficient As(V) removal by –FeOOH and –FeOOH/–MnO_2 embedded PEG-6-arm functionalized multiwall carbon nanotubes, Chem. Eng. Res. Des., 119 (2017) 75–86.

[S7] Z.J. Bajić, V.R. Djokić, Z.S. Veličković, M.M. Vuruna, M.Đ. Ristić, N.B. Issa, A.D. Marinković, Equilibrium, kinetic and thermodynamic studies on removal of Cd(II), Pb(II) and As(V) from wastewater using Carp (*Cyprinus Carpio*) scales, Dig. J. Nanomater. Bios., 8 (2013) 1581–1590.

[S8] Z.J. Bajić, Z.S. Veličković, V.R. Djokić, A.A. Perić-Grujić, O. Ersen, P.S. Uskoković, A.D. Marinković, Adsorption study of arsenic removal by novel hybrid copper impregnated tufa adsorbents in a batch system, Clean – Soil, Air, Water, 44 (2016) 1–12.

[S9] Z.S. Veličković, Z. Bajić, M. Ristić, A. Marinković, M. Vuruna, Modification of multi-wall carbon nanotubes for the removal of cadmium, lead and arsenic from wastewater, Dig. J. Nanomater. Bios., 8 (2013) 501–511.

[S10] M.K. Tiwari, S. Bajpai, U.K. Dewangan, R.K. Tamrakar, Suitability of leaching test methods for fly ash and slag: a review, J. Radiat. Res. Appl. Sci., 8 (2015) 523–537.

[S11] J.P. Gustafsson, Visual MINTEQ 3.0, beta, Available at: http://www.lwr.kth.se/English/ OurSoftware/vminteq/index.htm, Stockholm, Sweden, 2011.

[S12] W.D. Schecher, D.C. McAvoy, MINEQL+: User's Manual, Environmental Research Software, Edgewater, Hallowell, Maine, USA, 2001.

[S13] J.P. Stewart, Optimization of parameters for semiempirical methods V: modification of NDDO approximations and application to 70 elements, J. Mol. Model., 13 (2007) 1173–1213.

[S14] A. Pedretti, L. Villa, G. Vistoli, VEGA – An open platform to develop chemo-bioinformatics applications, using plug-in architecture and script programming, J. Comput.-Aided Mol. Des., 18 (2004) 167–173.

[S15] Z. Kolska, J. Matousek, P. Capkova, A new luminescent montmorillonite/borane nanocomposite, Appl. Clay Sci., 118 (2015) 295–300.

[S16] H. Zhu, X. Xiao, Z. Guo, X. Han, C. Zhou, Adsorption of vanadium (V) on natural kaolinite and montmorillonite:

characteristics and mechanism, Appl. Clay Sci., 161 (2018) 310–316.
[S17] R. Hojiyev, G. Ersever, I.E. Karaağaçlıoğlu, F. Karakaş, F. Boylu, Changes on montmorillonite characteristics through modification, Appl. Clay Sci., 127–128 (2016) 105–110.
[S18] N. Jović-Jovičić, Z. Mojović, M. Darder, P. Aranda, E. Ruiz-Hitzky, P. Banković, D. Jovanović, A. Milutinović-Nikolić, Smectite-chitosan- based electrodes in electrochemical detection of phenol and its derivatives, Appl. Clay Sci., 124–125 (2016) 62–68.
[S19] B. González, R. Trujillano, M.A. Vicente, A. Gil, M.N. Timofeeva, Two synthesis approaches of Fe-containing intercalated montmorillonites: differences as acid catalysts for the synthesis of 1,5-benzodeazepine from 1,2-phenylenediamine and acetone, Appl. Clay Sci., 146 (2017) 388–396.
[S20] Z. Petrović, P. Dugić, V. Aleksić, S. Begić, J. Sadadinović, V. Mićić, N. Kljajić, Composition, structure and textural characteristics of domestic acid activated bentonite, Contemp. Mater., 1 (2014) 133–139.
[S21] C. Ibarguren, P.M. Naranjo, C. Stötzel, M.C. Audisio, E.L. Sham, E.M.F. Torres, F.A. Müller, Adsorption of nisin on raw montmorillonite, Appl. Clay Sci., 90 (2014) 88–95.
[S22] B.A. Fil, C. Özmetin, M. Korkmaz, Characterization and electrokinetic properties of montmorillonite, Bulg. Chem. Commun., 46 (2014) 258–263.
[S23] A. Mitrović, M. Zdujić, Mechanochemical treatment of Serbian kaolin clay to obtain a highly reactive pozzolana, J. Serb. Chem. Soc., 78 (2012) 579–590.
[S24] Lj. Rožić, T. Novaković, S. Petrović, Z. Vuković, Ž. Čupić, Fractal analysis of physical adsorption on surfaces of acid activated bentonites from Serbia, Chem. Ind. Chem. Eng. Q, 14 (2008) 227–229.
[S25] A. Sdiri, M. Khairy, S. Bouaziz, S. El-Safty, A natural clayey adsorbent for selective removal of lead from aqueous solutions, Appl. Clay Sci., 126 (2016) 89–97.
[S26] K. Shameli, M.B. Ahmad, W.M.Z.W. Yunus, N.A. Ibrahim, Y. Gharayebi, S. Sedaghat, Synthesis of silver/montmorillonite nanocomposites using γ-irradiation, Int. J. Nanomed., 5 (2010) 1067–1077.
[S27] Y. Gao, N.R. Choudhury, N.K. Dutta, Systematic study of interfacial interactions between clays and an ionomer, J. Appl. Polym. Sci., 117 (2010) 3395–3405.
[S28] M.R. Soares, J.C. Casagrande, E.R. Mouta, Nickel adsorption by variable charge soils: effect of pH and ionic strength, Braz. Arch. Biol. Technol., 54 (2011) 207–220.
[S29] J.S. Markovski, V. Dokic, M. Milosavljevic, M. Mitric, A.A. Peric-Grujic, A.E. Onjia, A.D. Marinkovic, Ultrasonic assisted arsenate adsorption on solvothermally synthesized calcite modified by goethite, α-MnO_2 and goethite/α-MnO_2, Ultrason. Sonochem., 21 (2014) 790–801.
[S30] D. Budimirović, Z.S. Veličković, Z.J. Bajić, D.L. Milošević, J.B. Nikolić, S.Ž. Drmanić, A.D. Marinković, Removal of heavy metals from water using multistage functionalized multiwall carbon nanotubes, J. Serb. Chem. Soc., 82 (2017) 1175–1191.
[S31] Z.S. Veličković, A. Marinković, Z. Bajić, J. Marković, A. Perić-Grujić, P. Uskoković, M. Ristić, Oxidized and ethylenediamine-functionalized multi-walled carbon nanotubes for the separation of low concentration arsenate from water, Sep. Sci. Technol., 48 (2013) 2047–2058.
[S32] K. Taleb, J. Markovski, Z. Veličković, J. Rusmirović, M. Rančić, V. Pavlović, A. Marinković, Arsenic removal by magnetite-loaded amino modified nano/microcellulose adsorbents: effect of functionalization and media size, Arabian J. Chem., 12 (2019) 4675–4693.